A subsurface record of the Lower Jurassic of the Roer Valley Graben, Belgium

Laia Real Malats

Supervised by:
Dr. João P. Trabucho Alexandre
Mateus Kroth

Abstract

The Upper Triassic – Lower Jurassic in the Molenbeersel borehole is represented by the Sleen (Rhaetian) and Aalburg formations (Hettangian to Pliensbachian) of the Altena Group. Deposition took place in the Roer Valley Graben, a Cimmerian Basin formed by tectonic differentiation during the early Cimmerian phase. Throughout the Upper Triassic – Lower Jurassic, the Laurasian Sea occupied the northwest of Europe; it was a shallow marine epeiric sea that connected the Boreal Arctic Sea to the north and the Tethys Sea to the south. The presence of the Altena Group varies in the Cimmerian basins due to differential subsidence and posterior erosion, which makes its study complex. This project presents the first sedimentological characterization of the Sleen and Aalburg formations in the Belgian subsurface, including lithological features, mineralogical data, $\delta^{13}C_{org}$, total organic carbon (TOC), and sulfur data. The formations consist of dark argillaceous mudstones with ironstone horizons and concretions. The different sedimentary structures (small-scale cross-lamination, bioturbation…) and authigenic minerals (pyrite and siderite) of the deposits indicate a dynamic setting between oxygenated bottom waters to dysoxic – anoxic –euxinic conditions. A comparison between the Sleen and Aalburg formations in the Roer valley Graben and the Cleveland Basins (Lias Group), UK, opens the possibility of the presence of the Pliensbachian – Toarcian boundary in the Molenbeersel borehole.

Keywords: Upper Triassic - Lower Jurassic boundary, Roer Valley Graben, mudstones, ironstones, Laurasian Sea.

Acknowledgments

I would like to express my gratitude, in first place, to João Trabucho Alexandre, the supervisor of my master thesis. Thank you for giving me the opportunity to discover this new area of sedimentary geology and offering me the chance to learn new techniques and work with different people on a topic that I would not expect to find so interesting and challenging. Thank you for making me more active in my research and allowing me to learn from your knowledge. I want to thank you for all the opportunities, outside of this project as well, that you have offered me. Last year, when I arrived to Utrecht, I was quite unmotivated with my studies here and struggled to find my pace. Participating in your course "Applied Stratigraphy and Subsurface Basin Analysis" really helped me find my spot at this university and made me want to do my master's thesis under your supervision. It really made a huge impact in my first few months here. Thank you again for this great opportunity and I hope to keep in contact. This would not have been possible without your support.

Mateus, thank you very much for all the support that you have offered me this year, having you as a second supervisor has really made a difference during the thesis. Thank you for the weekly meetings, the advice, and the commitment to the project. But also, thank you for the laughs, the coffee breaks, the climbing weekends, and the moments that really made this 2nd year of my master light and fun. I hope to not only see you in research meetings and conferences in the future, but also in trips outside-of-academia in Spain soon.

I also want to thank all the people that have participated in this project: thank you Anita van Leeuwen-Tolboom and Coen Mulder for all the help in the lab, for teaching me and having the patience to explain to me how to apply the techniques in a professional and safe way. Thank you, Coen, for making me feel supported and accompanied during long evenings at the lab. Thank you Bejanim Gill and Rachel Reid from Virginia Tech University for making it possible to study the geochemical data of this project.

I have very much enjoyed forming part of the Sedi team this year. Thank you Pelle, Joris, Mutaz, and Mariana for making me feel welcome in the group and for the interesting and funny moments at VMA. Even if it was a "short" stay with you, it really made me feel part of the group in a very warm way.

A very big thank you to Andrew, Rachel, Celia, Aliss, Mariana, Edgar, Marijn, Maria, among many other friends, for being my family in Utrecht. I cannot imagine my life here and being where I am without you. Thank you for all the support and love you have showed me throughout these 2 years. Thank you for the laughs, the trips, and for being there during hard times. I truly believe that these friendships do not end here and I am excited to meet you in Madrid. I am really going to miss you. I also thank my friends from Madrid, that too have listened to me talk about my thesis and life here, and that have come to visit me and made me feel like home. I love you.

I also need to thank my parents, Núria and Paco, this would have definitely not been possible without you. I cannot thank you enough for all the support, in all the possible ways. Thank you for giving me the opportunity to come to Utrecht to study, for always encouraging me to learn and live, and for engaging with my studies from the beginning. Thank you for being part of these 2 years here, even from a distance. Us estimo.

Finally, I would like to thank me, for not quitting during very hard times and trying to find the positive side of my life here. I thank myself for being able to meet many people, make great friends, learn more than what I expected, and finish this master being very proud of the life I built here in Utrecht, academically and personally.

Table of contents

List of figures

and calcite nodules are present throughout the cores (except the lowermost interval). Macrofossil content is present, characterized by ammonites, gastropods, echinoderms, and bivalve bioclasts, they are found pyratized in some areas. Oxidized organic matter is also present. Grain size scale: fm, fine mudstone; mm, medium mudstone; cm, coarse mudstone.

Figure 11. The deposits of the Lower Jurassic of the Molenbeersel borehole. **A)** Breccia located at the top of the lowermost interval where mudstone and ironstone clasts can be observed between the depths of 1717.63 - 1717.40 mbs. **B)** Example of the deposits of the uppermost interval: septarian ironstone and mudstones between the depths of 1287.61 - 1287.44 mbs. We observe that the boundaries of the ironstone is well observed. **C)** Contact between the Cretaceous (lighter color) and the Lower Jurassic (darker color) at a depth of 1283.12 mbs.

Figure 12. Example of the fossil and bioturbation content of the Lower Jurassic in the Molenbeersel borehole. **A)** Example of a burrow (white arrow) in the lowermost interval of the core at 1718.84 mbs. The burrow presents pyritization in the interior part of the bioturbation. **B)** Example of a pyritized bioturbation (white arrow) at 1310.64 mbs**. C)** Example of oxidized organic matter (white arrow) at 1313.7 mbs.

Figure 13. Color analysis of the Molenbeersel borehole with the red (700WL) and green (550WL) color data. In the curve including ironstones (middle), we observe that the main peaks (higher for the 700WL; lower for the 550WL) correspond to the ironstone horizons and concretions. When removing the peaks, the curves present a more homogenized trend. The 550WL green does not present important shifts. The 700WL red curve presents minor changes and an interval of lower values without smaller shifts between 1291 – 1280 mbs.

Figure 14. XRD results of the different deposits from the Molenbeerel core. **A)** Represents the XRD results of Group 1, which includes all the mudstone samples of the upper and middle interval (1227.01 - 1511.72 mbs). The main minerals identified are quartz, clay minerals (14, 10, and 7 Å spacing), chamosite, pyrite, and albite. **B)** Represents the XRD results of Group 2, which includes the ironstones from the uppermost interval. The ironstones are composed mainly of siderite, quartz, calcite, and clay minerals (10 and 7 Å spacing). **C)** Represents the XRD results of Group 3, which includes the one sample analyzed from the lowermost interval. The main minerals are pyrite, quartz, and kaolinite (7 Å spacing clay mineral).

Figure 15. Relative mineral changes (%) throughout the core. The main minerals identified have been plotted to observe general trends throughout the core. The quartz is the dominant mineral for the mudstones in all the samples. The trend of the quartz and the kaolinite (7 Å *d* spacing clay mineral) and the 10 Å *d* spacing clay mineral, present very similar tendencies in the lower part of the uppermost interval of the core (1283.15 - 1313.9 mbs). The trend of the clay minerals remains the same in the upper part, but the quartz content presents more variations. The pyrite content slightly shifts but remains rather low throughout the core.

Figure 16. Lithofacies characterization of the Molenbeersel borehole. **A)** Example of lithofacies 1 (LF1) with massive appearance (1288.70 mbs). **B)** Example of LF1 from above with very fine mudstone and no fossil or bioturbation content (1305.3 mbs). **C)** Example of LF1 with an ammonite fossil marked with a white arrow (1305.70 mbs). **D)** Example of lithofacies 2 (LF2), with coarser grain size (1310.62 mbsf). Oxidized organic matter is also present in this sample. **E)** Example of LF2 where the primary lamination has been deformed due to the growth of the ironstone nodule with internal calcite veins (1296.68 mbsf). **F)** Example of septarian ironstone (1313.9 mbsf). Legend: Black: LF1; Grey: LF2. Grain size scale: fm, fine mudstone; mm, medium mudstone; cm, coarse mudstone.

Figure 17. Microfacies location in the Lower Jurassic of the Molenbeersel borehole next to the log. Microfacies 1: massive to slightly laminated fine mudstone. Microfacies 2: Fine to medium mudstone, with lamination and bed surfaces. Microfacies 3: Bioclastic fine mudstone. Microfacies 4: Massive to laminated, medium to coarse mudstones. Microfacies 5: Medium to coarse mudstone, with lamination and bedding surfaces. Microfacies 6: Ironstones.

Figure 18. Plane-polarized-light optical micrographs of the Lower Jurassic in the Molenbeersel borehole and microfacies characterization**. A)** Example of MF1 with a massive appearance in fine-mudstones (MB41, 1291.15 mbs). Py: pyrite. **B)** Example of MF2, erosive bed surface with detrital quartz and bioclast silt-size grains lag (yellow dashed lines) and bioclasts (MB69, 1296.75 mbs). **C)** Example of MF3, burrow with fecal pellet accumulation and calcite cement, indicating early cementation (white arrow) (MB102, 1303.94 mbs). **D)** Example of MF4, coarser grain size compared to the prior microfacies can be observed with a discontinuous lamination. Pyrite (Py, arrow) in larger aggregates and framoidal and ehuedral forms (MB52, 1293.25 mbs). **E)** Example of MF5 with an erosive bed surface with an accumulation of quartz and biolcast detrital grains lag (yellow dashed line).

Normal grading can be observed (Symbol) (MB18, 1286.55 mbs). **F)** Example of MF5 where three bed surfaces can be observed (dashes yellow lines); the lower and middle planes present a normal grading trend (Symbol). The uppermost bed plane presents a change to coarser grain size (MB26, 1288.15 mbs).

Figure 19. Plane-polarized-light optical micrographs of the Lower Jurassic in the Molenbeersel borehole. **A)** Example of an ammonite bioclast (white arrow), pyrite (Py), and quartz silt size grains from MF4 (MB9, 1285.75 mbs). **B)** Example of organic matter with an orange color (white arrow) (MB13, 1285.55 mbs). The unflattened shape indicates early cementation. **C)** Example of an ironstone concretion with a very fine grain size that contains articulated bivalve shells from MF6 (Mb26, 1288.15 mbs). **D)** Example of horizontal lamination where authigenic pyrite framboidal grains (Py) follow the primary lamination in MF1 (MB115, 1306.19 mbs). **E)** Example of echinoderms (white arrow) and gastropod from MB3 (MB152, 1313.60 mbs). **F)** Example of pyrite aggregate (Py) and veins from MF4 (MB9, 1285.75 mbs).

Figure 20. $\delta^{13}C_{org}$, TOC and Sulfur record of the Lower Jurassic of the Molenbeersel borehole. The figure presents five curves. Dark blue: TOC data complete, where two positive anomalies can be observed: 1) upper interval due to the presence of ironstones; 2) in the lowermost interval where ironstones are not present. Light blue: TOC data without the ironstone peaks. More shifts can be distinguished but still, a rather stable trend can be observed. Orange: Sulfur data complete, higher variability is observed in all three intervals. Pink: Sulfur data without the ironstone values. Heterogeneous trend, many of the positive peaks remain after removing the ironstone peaks. A major shift is present in the lowermost interval, but reaching deeper depths than the TOC excursion. Green: $\delta^{13}C_{org}$ complete, where the data presents rather stable values with the exception of the lowermost interval.

Figure 21. Relationship between the TOC and sulfur data of the deposits of the Lowe Jurassic of the Molenbeersel borehole. The R^2-value that provides information about the correlation between both variables presents a lower association, indicating a non-linear relationship between the TOC-sulfur data. The record has been grouped into four groups: grey-uppermost interval, yellow-mid interval, pink-lowermost interval, and red, ironstones. As we can observe, the ironstones present a high range of sulfur values but similar TOC values, similar to what can be observed for the mudstones of the uppermost interval (with lower TOC values). The mid-interval presents similar values of

TOC and some variation in sulfur, but compared to the uppermost interval the values are more homogenized. The lowermost interval presents the highest variability represented by either high TOC – high sulfur data points or; low TOC – and variable sulfur values.

Figure 22. Lithostratigraphic proposal**,** lithological features, gamma ray (black), TOC (blue), sulfur (orange), $\delta^{13}C_{org}$, (darker green), and spectrophotometry (WL550- light green, WL700-red) of the Molenbeersel core. The gamma ray and color data are only available for the uppermost interval. The lithostratigraphic proposal is based on lithological features and TOC data. The Sleen Formation (Triassic) does not present ironstones. Furthermore, it presents a TOC anomaly, that is characteristic of the Triassic – Jurassic boundary. The Aalburg Formation is characterized by mudstones with siderite ironstones. The TOC shifts represent the ironstones.

Figure 23. Geochemical proxy records of environmental changes across de Triassic-Jurassic boundary at the Kuhjoch section, Eiberg Basin (Austria). (a) The organic C-isotope signature [‰], (b) Total Organic Carbon content [%] (Modified from Ruhl & Kürschner, 2010).

Figure 24. New proposal on the age of the Molenbeersel deposits of this project. Marked with a red rectangle are the changes for the lowermost interval (1717.6 - 1720.37 mbs) from Lower Jurassic to Late Triassic (Modified from Edwin Maes, 1990).

Figure 25. Different sedimentary structures and components of the Lower Jurassic of the Molenbeersel borehole. **A)** Small-scale cross lamination, the cross-bedding geometry is indicated with dashed yellow lines (MB36; 1290.15 mbs**). B)** Small-scale ripple, it is possible to distinguish it due to the contrast between grains, indicated with a yellow dashed line (MB146; 1312.40 mbs). **C)** Calcite concretion in the lower-right corner, presenting a smaller grain size and a lighter color. Unflatten organic matter with an orange color, indicated by a white arrow; indicates early cementation (MB13; 1285.55 mbs**). D)** Pyrite aggregate confirmed by smaller framboidal pyrites (MB69; 1296.75 mbs). **E)** Sharp edges of a bioclast; indicative of little transport from the source area (MB69; 1296.75mbs). **F)** Pyrite growth inside an ammonite bioclast, the original internal structure is not preserved (MB9; 1284.75 mbs).

Figure 26. TOC, sulfur, and color data (WL550, WL700) of the uppermost interval (1283.15 - 1313.9 mbs) of the Lower Jurassic at the Molenbeersel borehole. The red highlight indicates the matching peaks of the WL700 (red)

and TOC data. The orange highlight indicates the non-matching peaks between the same two variables; this is interpreted to be explained by the sampling selection.

Figure 27. Stratigraphical framework for the Lower Jurassic Lias Group in the Cleveland Basin (after Powell 1984; Knox 1984; Rawson & Wright 2000) and the Belgium – Netherlands nomelanclature used in the Roer Valley Graben (After Adrichem Boogaert & Kouwe, 1994–1997; Herngreen et al., 2003).

Figure 28. Stratigraphic log of the studied section of Dove's Nest core (left) and of the correlative composite outcrop section along the North Yorkshire coast between Hawsker Bottoms and Port Mulgrave (right; Fig. 1). Organic carbon isotopes ($\delta 13C_{org}$) and whole-rock total organic carbon (TOC_{WR}) profiles are shown with their correlation. Grain size scale: fm, fine mudstone; mm, medium mudstone; cm, coarse mudstone; fs, very fine sandstone. Yorkshire coast 'bed' numbers from Port Mulgrave after Howarth (1962, 1992); named marker beds after Howarth (1955).Dove's Nest data from this study. Yorkshire coast δ13Corg data from Hawsker Bottoms: orange, Littler et al. (2010); blue, Cohen et al. (2004); pink, Kemp et al. (2005). Port Mulgrave: green, Kemp et al. (2005); red, Cohen et al. (2004). Saltwick Bay: cyan, Cohen et al. (2004). TOC data for the Yorkshire coast are composite section values after McArthur (2019; thick line with unfilled circles) and Kemp et al. (2011; thin grey high-resolution curve). Abbreviations of biostratigraphic zonation: Tenui. = Tenuicostatum; Spin. = Spinatum; Exa. = Exaratum; D. s. = Semicelatum; * = Tenuicostatum; † = Clevelandicum; P. p. = Paltum; P. h. = Hawskerense; P. a. = Apyrenum; Gib. = Gibbosus; A. s. = Subnodosus (Trabucho-Alexandre et al., 2022).

List of tables

1. Introduction

The Jurassic of Flanders, Belgium, lies buried in the subsurface and it has great importance for the correlation between the outcrops of Great Britain and the west of continental Europe (Trabucho-Alexandre et al., 2022). The Jurassic rocks were deposited in the Laurasian epeiric Sea, which connected the Boreal Sea to the north, with higher siliciclastic input, to the Tethys Ocean in the south, which had a warmer climate and more carbonate deposition (Doornenbal & Stevenson, 2010).

The Lower Jurassic in Flanders, as is the case in the Netherlands, is geographically limited to Cimmerian basins, which underwent differential subsidence during the early Cimmerian tectonic phase (Anisian – Ryazanian), related to the opening of the Atlantic Ocean. The Cimmerian basins underwent two major erosive events, the first one during the Middle-Upper Jurassic, and the second one during the Upper Cretaceous tectonic inversion (Demyttenaere, 1989). Hence, the Jurassic does not present a continuous record and its study is challenging.

The Roer Valley Graben is a Cimmerian basin that offers a great opportunity to study the deposits of the Lower Jurassic in the Laurasian Sea setting, since its sedimentary characterization has not been studied in detail. Additionally, it can provide insights into the connection between Belgium, the Netherlands, and the UK since there is a lack of information in this topic on the scientific community. The Roer Valley Graben is a mid-Mesozoic rift asymmetric system developed during the tectonic differentiation of the Southern Permian Basin during the early Cimmerian phase (Ziegler, 1988; Zijerveld et al., 1992; Deckers et al., 2021). Due to the tectonic phases that the Roer Valley Graben experienced, the geographic distribution of the deposits is rather discontinuous (Ziegler, 1988; Zijerveld et al., 1992; Winstanley, 1993; Geluk et al., 1995).

This project offers a stratigraphic and sedimentological insight of the 36 m of Upper Triassic and Lower Jurassic rocks obtained in the Molenbeersel borehole by the Geological Survey of Belgium deposited in the Roer Valley Graben, northeast Flanders, Belgium (Fig. 1). The succession consists of dark argillaceous mudstones with red ironstones in nodules and concretionary horizons as well as calcareous concretions throughout the whole succession.

In this project, I suggest that the Sleen Formation (Rhaetian) and the Aalburg Formation (Hettangian - Pliensbachian) from the Altena Group are present in

the Molenbeersel borehole by the study of sedimentological features, mineralogical data, $\delta^{13}C_{org}$, TOC, and sulfur data.

These formations can be correlated with the outcrops described in the UK (Powell, 2010 and references therein). The deposits in the Molenbeersel borehole are rather homogeneous and finer-grained compared to the Aalburg Formation in other Cimmerian Basins from the Netherlands and the corresponding formations in the Cleveland basin, which display more variability in the grain size and sedimentary structures (Powell, 2010; Trabucho-Alexandre et al., 2012, 2022). These features could indicate a slightly different paleodepositional setting in comparison with other basins (Trabucho & Wang, 2024).

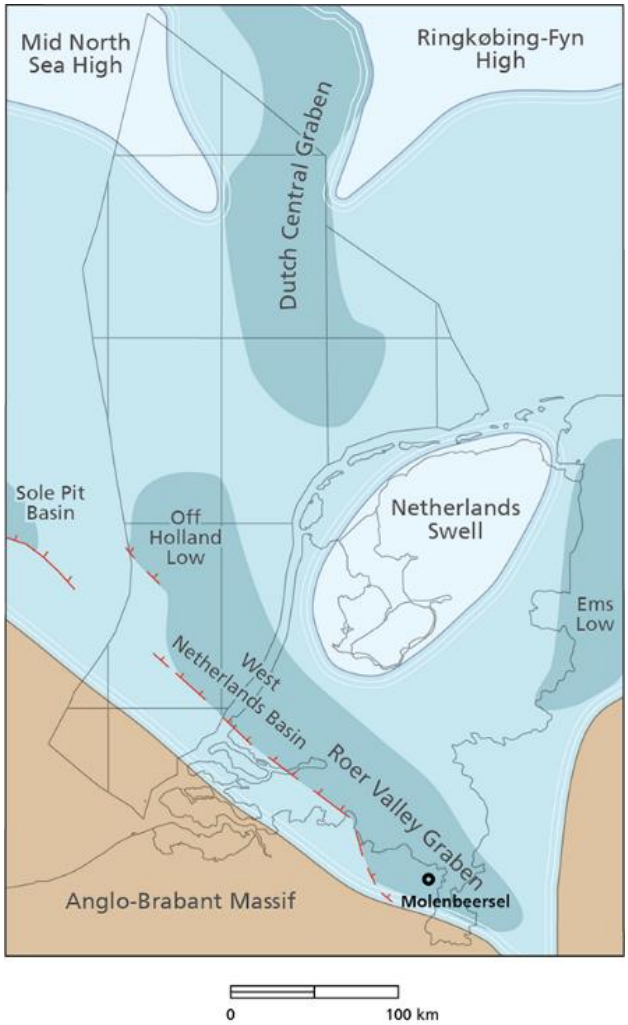

Fig 1. Paleogeographic map of the area where the core was obtained (Molenbeersel) during the Lower Jurassic. (J. P. Trabucho-Alexandre & Wong, 2024)

2. Geological setting

2.1. Roer Valley Graben

The Roer Valley Graben is located in the southern part of the Netherlands, north Belgium, and West Germany. It forms the northwest branch of the European Cenozoic Rift system (Ziegler, 1992). The Roer Valley Graben formed during extensional tectonic phases that took place during the late Permian to Triassic, called the Cimmerian phases (Ziegler, 1992; Zijerveld et al., 1992; Luijendijk et al., 2011). The Roer Valley Graben is limited by the Campine Basin in the southwest, the Peel Block in the northeast, and the West Netherlands Basin in the northwest (Ziegler, 1992; Zijerveld et al., 1992; Geluk et al., 1994; Luijendijk et al., 2011; Deckers et al., 2021).

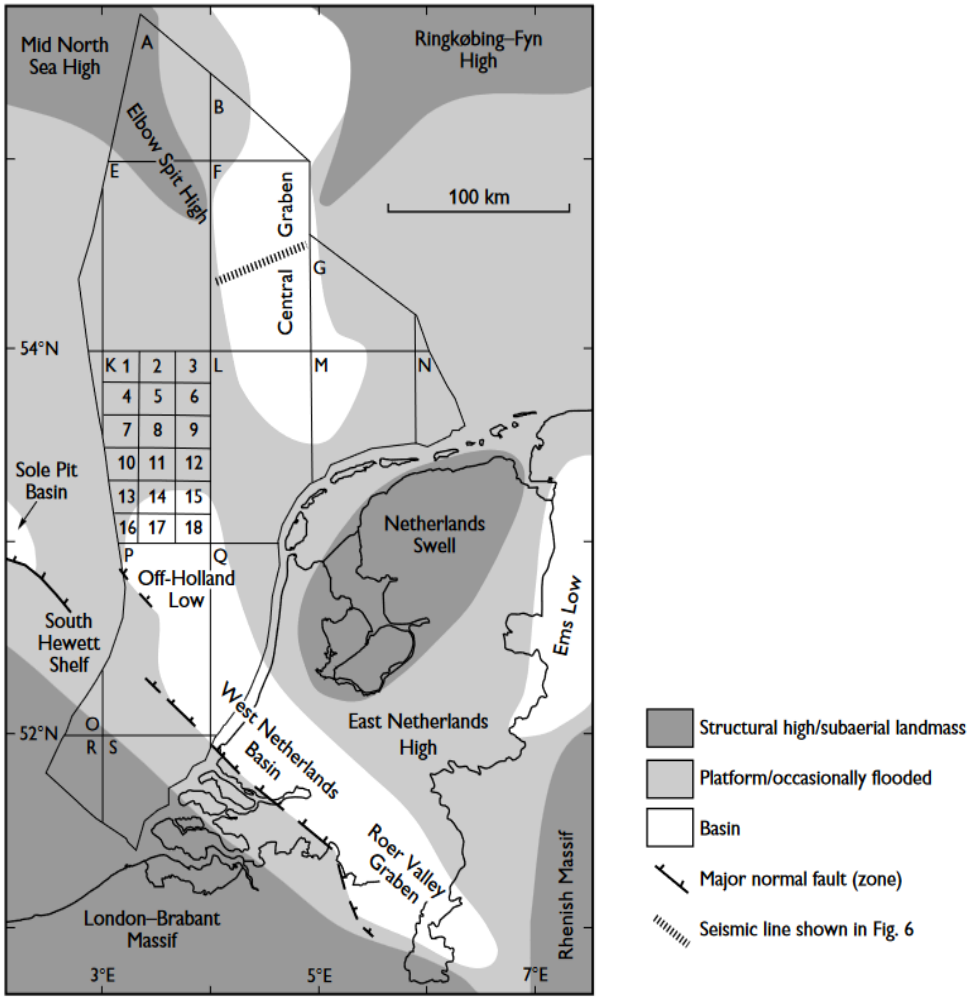

Fig 2. Main structural elements during the Late Triassic to Early Jurassic in the Netherlands and North of Belgium (Modified from van Adrichem Boogaert & Kouwe, 1994–1997).

2.2. Geological evolution of the Roer Valley Graben

During the Upper Paleozoic (Permian), the Roer Valley Graben was part of the Southern Permian Basin, a single and extensive basin (Ziegler, 1990; Ondrak et al., 1999; Worum et al., 2005). During the opening of the Atlantic Ocean, the Southern Permian Basin was differentiated and subside into smaller basins/blocks (Anisian-Ryazanian) (Ziegler, 1990; Geluk et al., 1994; Ondrak et al., 1999; Worum et al., 2005; Deckers et al., 2021). The tectonic pulses that led to the individualization of the smaller basins are called the Cimmerian phases (Ziegler, 1990; Herngreen et al., 2003). The extension can be divided into four sub-phases: Hardegsen (Early Triassic), early Cimmerian (Anisian–Carnian), middle Cimmerian (Aalenian–Callovian/Oxfordian), and late Cimmerian (Kimmeridgian–Ryazanian) (Geluk et al., 1995; Herngreen et al., 2003). The Roer Valley Graben individualized during the early Cimmerian phase (Fig. 3).

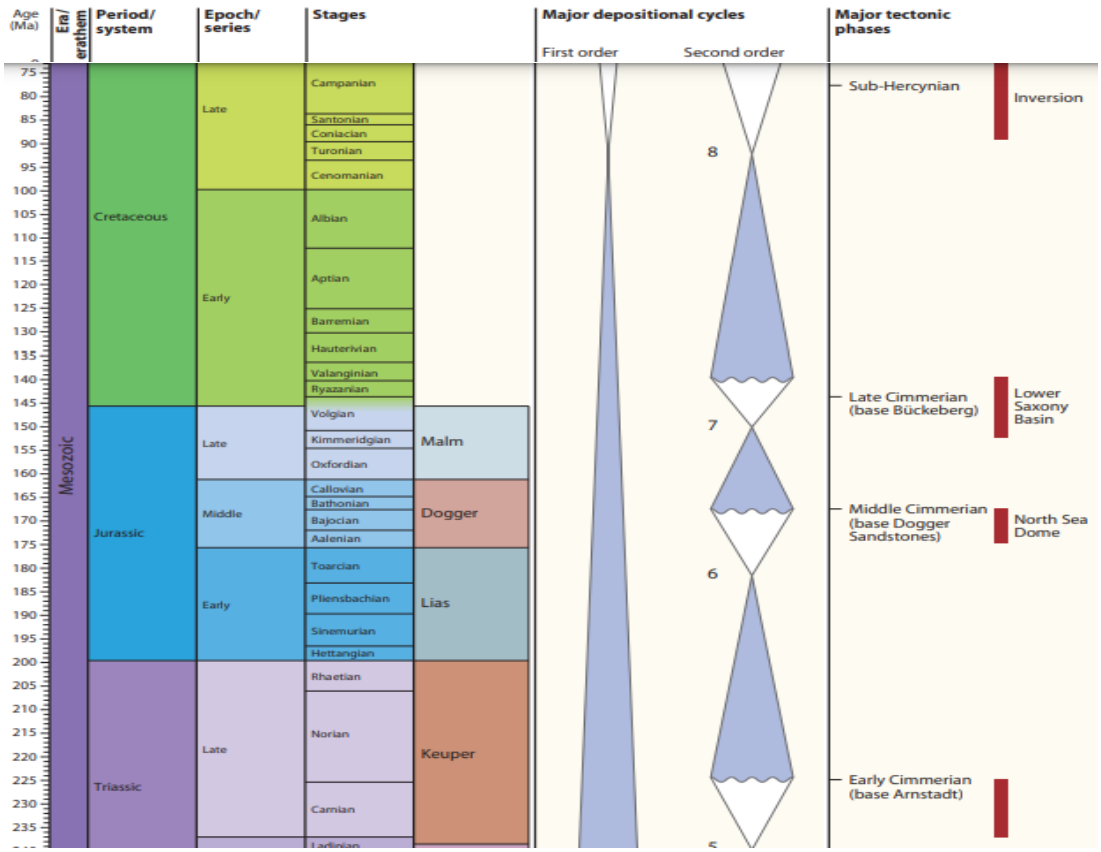

Fig 3. Triassic to Cretaceous timescale with tectonic episodes and major depositional sequences in the South Permian Basin area (Modified from Pharaoh, T.C et al., 2010).

During the Rhaetian (Upper Triassic), a major transgressive pulse took place, shifting from a continental to a marine setting (Herngreen et al., 2003). A shallow epeiric sea established, the Laurasian Sea, connecting the Boreal Arctic Sea to the north, characterized by a higher siliciclastic input, to the Tethys Ocean to the south, with a warmer climate and carbonate production (Ziegler, 1990; Callomon, 2003; Wong, 2007; Lott et al., 2010). The Laurasian Sea extended from the present-day UK, Netherlands, Belgium, Germany, and Poland (Lott et al., 2010). During the Toarcian, a more restricted basin circulation took place leading to anoxic bottom waters setting (Herngreen et al., 2003; Wong et al., 2007; Lott et al., 2010).

A gradual uplift in the northern part of the South Permian Basin area took place during the middle and late Cimmerian phases leading to an important structural differentiation and a non-depositional setting or erosion of some Lower Jurassic deposits (Herngreen et al., 2003; Lott et al., 2010). In the southern Cimmerian Basins, the uplift did not have a great effect and marine deposition continued until the Oxfordian (Herngreen et al., 2003*;* Lott et al., 2010). The marine sedimentation stopped and the deposits from late Oxfordian to early Kimmeridgian show an unconformity (Herngreen et al., 2003). Differential subsidence continued, leading to the deposition of lacustrine and alluvial plain deposits. During the Late Cretaceous, tectonic inversion took place, eroding part of these deposits of the Cimmerian basins (Herngreen et al., 2003; Lott et al., 2010).

2.3. Lithostratigraphic background

The Lower Jurassic of the Roer Valley Graben has been subdivided following the same nomenclature as the Netherlands (NAM & RGD, 1980; van Adrichem Boogaert & Kouwe, 1994; Lott et al., 2010). The Upper Triassic - Lower Jurassic is represented by the Altena Group, deposited between the Rhaetian to Oxfordian (NAM & RGD, 1980; van Adrichem Boogaert & Kouwe, 1994; Lott et al., 2010). The deposits are characterized mainly by dark argillaceous to calcareous epeiric-neritic mudstones, sandstones, marls, and limestones that can reach around 1600 m of thickness in some basins (Herngreen et al., 2003**,** J. P. Trabucho-Alexandre & Wong, 2024). The Altena Group can be subdivided into five formations: Sleen, Aalburg, Posidonia Shale, Werkendam and Brabant (NAM & RGD 1980; Van Adrichem Boogaert, H.A. & Kouwe, W.F.P. 1994) (Fig. 4).

The Sleen Formation is characterized by grey fossiliferous mudstones and claystones. The thickness can reach around 20-45 m in the Roer Valley Graben (NAM & RGD, 1980; van Adrichem Boogaert & Kouwe, 1994; Dusar et al., 2001). Deposited in shallow and open-marine environments during the Rhaetian (Legrand, 1961). Overlies the Keuper or the Muschelkalk Formation from the Triassic (Upper - Mid Triassic) (NAM & RGD, 1980; van Adrichem Boogaert & Kouwe, 1994).

The Aalburg Formation is composed of black argillaceous to calcareous mudstones. It represents a marine transgression (Lott et al., 2010 and references therein). Ammonites, belemnites, and mollusks are found in pyritized form. Siderite concretions are common throughout the formation (Dusar et al., 2001). Thickness can reach up to 700 m, but variations are due to subsidence and erosion patterns. The Aalburg Formation was deposited in a shallow to open-marine, neritic environment during the Hettangian to Pliensbachian (Legrand, 1961; van Adrichem Boogaert & Kouwe, 1994). It lies over the Sleen Formation and lies under the Posidonia Shale Formation. In the Roer Valley Graben, the upper surface has been eroded the Upper Cretaceous Chalk Group overlaps (NAM & RGB, 1980; van Adrichem Boogaert,. & Kouwe, 1994; J. P. Trabucho-Alexandre & Wong, 2024).

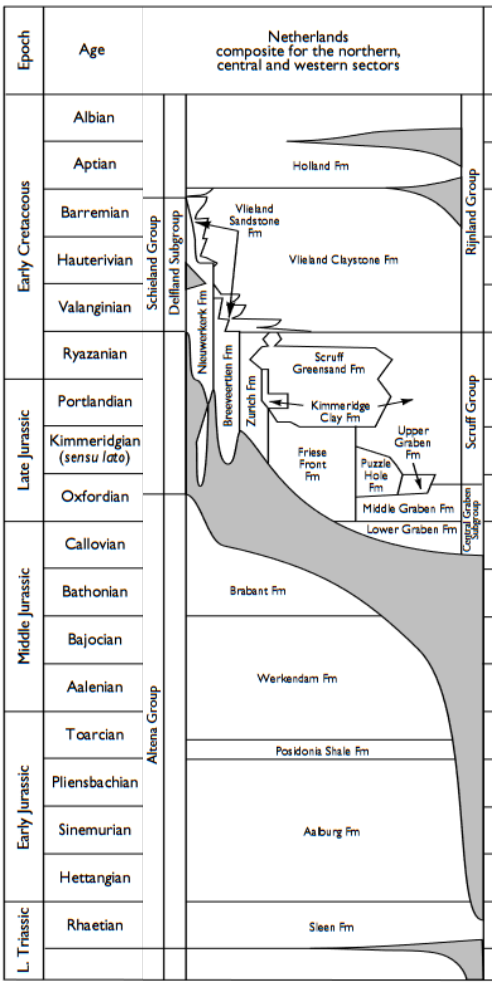

The Posidonia Shale Formation is formed by dark carbonaceous mudstones with carbonate beds. Deposited in stagnant water conditions under anoxic environments above storm wave base during the early Toarcian (NAM & RGD, 1980; van Adrichem Boogaert & Kouwe, 1994; Dusar et al., 2001).

Fig. 4. Regional lithostratigraphic chart of the Upper Triassic – Lower Cretaceous for the Netherlands and north Belgium (Modified from van Adrichem Boogaert &

Kouwe, 1994–1997; Herngreen et al., 2003).

2.4. Lower Jurassic in West Europe

The Jurassic of Flanders, Belgium has an important role for the lithostratigraphy correlation and dynamics of the deposits of the Laurasian Sea (Netherlands, UK…) since there is a link missing between the different basins conforming the Laurasian Sea area (Lott et al., 2010).

2.4.1. The Netherlands

As has been mentioned, the Netherlands and Flanders share the same lithostratigraphic nomenclature and similar lithological features of the deposits. Some of the Cimmerian basins found in the Netherlands are the West Netherlands Basin, the Campine Block, and the Dutch Central Graben (NAM & RGD, 1980; Ziegler, 1992; Zijerveld et al., 1992; van Adrichem Boogaert & Kouwe, 1994; Dusar et al., 2001).

2.4.2. United Kingdom (UK)

The Lower Jurassic deposits of the UK have been extensively studied due to the good access to the outcrops. In this project I compared the Molenbeersel deposits to Lower Jurassic of the Cleveland Basin (Wilson et al., 1934; Rawson & Wright, 1992, 1996; Powell, 2010) (Fig. 5).

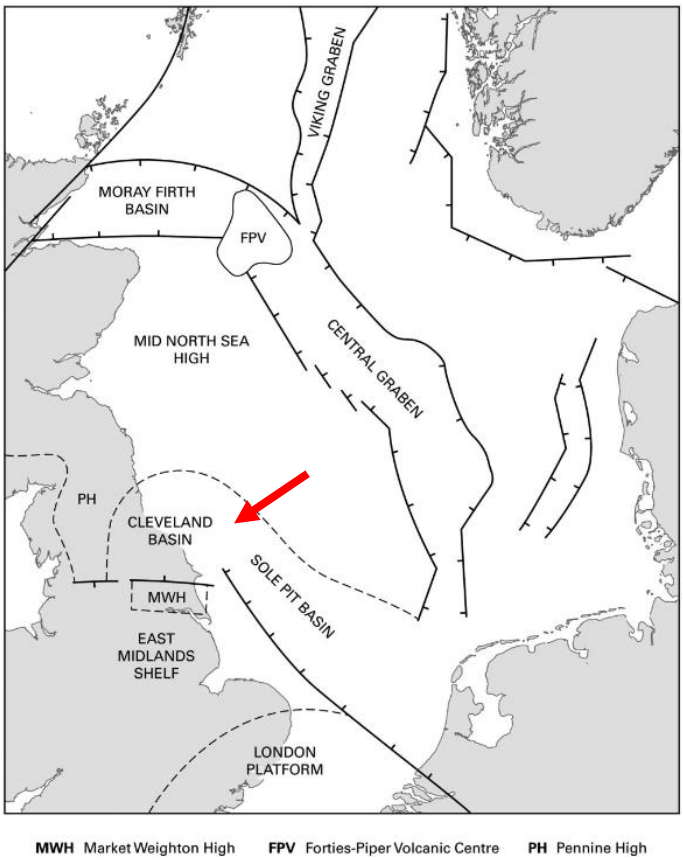

Fig. 5. Generalized paleogrepgraphical setting during the Jurassic. The Cleveland Basin is marked with a red arrow (after Knox et al., 1991).

The Upper Triassic (Rhaetian) is represented by the Penarth Group (Benfield & Warrington, 1988; Ivimey–Cook & Powell, 1991), and the Lower Jurassic by the Lias Group (O'B Knox, 1984; Powell, 1984; Ivimey–Cook & Powell, 1991; Rawson & Wright, 1992) (Fig. 6).

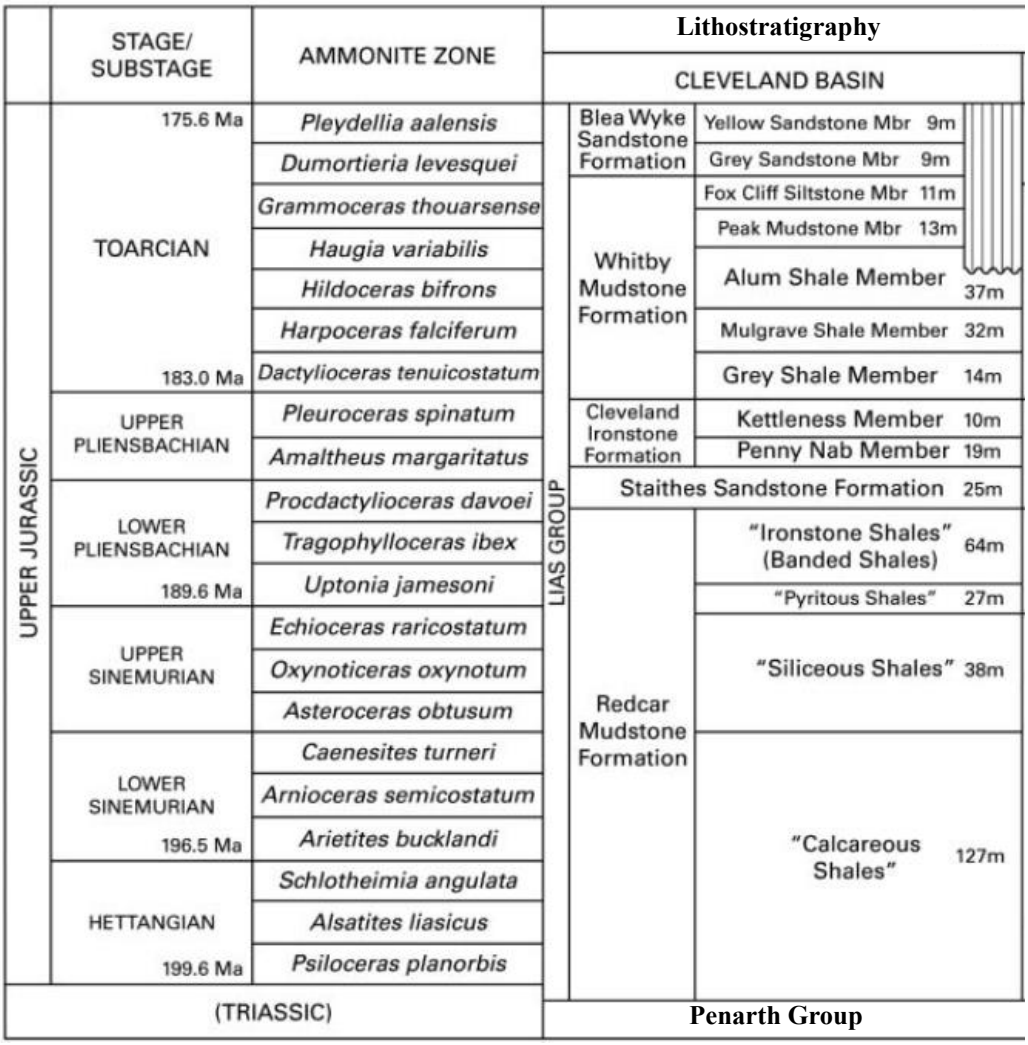

Fig. 6. Lithostratigraphical framework for the Lower Jurassic Lias Group in the Cleveland Basin and their average thickness (after Powell 1984; Knox 1984; Rawson & Wright 2000). Ages (Ma) are from Ogg et al. (2008).

3. Material and methods

3.1. The Molenbeersel borehole

The Molenbeersel borehole was drilled in June 1990 by the Belgium Geological Survey (Edwin Maes, 1990). Universal Transverse Mercator (UTM) coordinates 51 ° 10' 20. 3"N; 05° 45' 59.16"E.

The Lower Jurassic deposits comprise approximately ~ 500 m, which 36 m of the total have been recovered. Three different depth intervals from the Lower Jurassic were acquired: 1283.15 - 1313.9 meters below surface (mbs); 1510.1 - 1511.72 mbs and, 1717.6 - 1720.37 mbs. From 1227.01 to 1282.73 mbsf (Edwin Maes, 1990). Figure 7 shows the Molenbeersel borehole and the recovered intervals obtained by the Belgium Geological Survey; the three red arrows indicate the three intervals studied in this project and the initial age given by the Belgium Geological Survey.

The drilling process took place in 5 phases: the first two phases were conducted by a full-bore. The 3rd and 4th phases until the depth of 1313.90 m, the cores have a diameter of 85 mm. The 5th phase was operated until the depth of 1772.01 m with a core size of 63.5 mm (Edwin Maes, 1990).

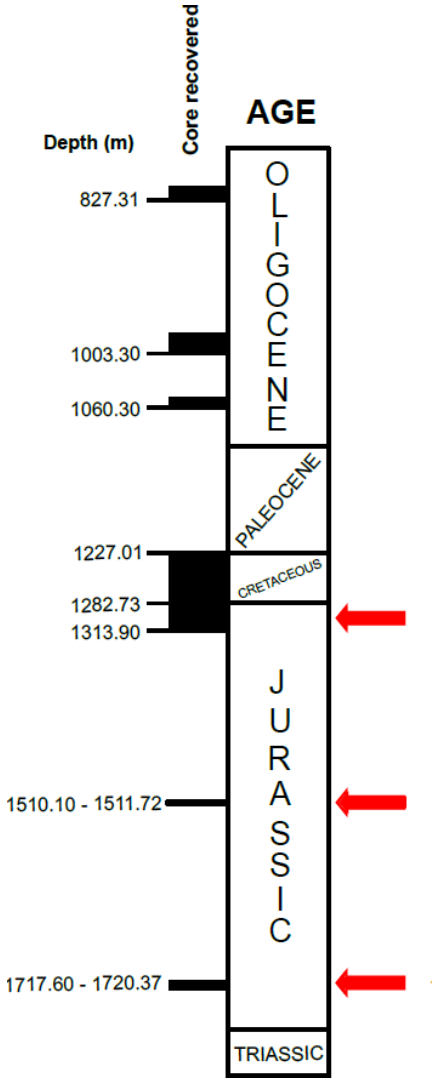

Fig. 7. Technical drilling scheme of the Molenbeersel borehole. The three red arrows indicate the recovered material that was studied in this project (Modified from Edwin Maes, 1990).

3.2. Sampling strategy

A total of 179 samples were collected between the 21st of March and the 17th of May 2023. I used a hammer to collect a quarter to half a barrel. The spacing between the samples was established every 20 cm interval to obtain a good overview of the Lower Jurassic between the depths of 1282.73 mbs and 1720.37 mbs.

From the uppermost interval (1283.15 - 1313.9 mbs), I collected 154 samples. From the mid-interval (1510.1 - 1511.72 mbs), 9 samples and, from the lowermost interval, 16 samples were collected. The sample distribution is shown in Figure 8.

3.3. Sedimentological analysis

3.3.1. Logging strategy

A description was performed with a scale of 1:20 on the unsliced surface of full barrels (Fig. 8). The characterization includes primary and secondary structures, such as rock fabric, texture, composition, color, bioturbation intensity, and macrofossil content. The log was subsequently digitalized using Illustrator.

Lowermost interval
1717.6 - 1720.37 mbsf

Middle interval
1510.1 - 1511.72 mbsf

Uppermost interval
1283.15 - 1313.9 mbsf

Cretaceous

Fig. 8. Sample distribution for the thin sections and XRD analysis samples (yellow dots) and the fossil sample (light blue dots). The three depth intervals are separated in boxes as the legend indicates. In the top right sample box, we can observe the contact between the Cretaceous Chalk Group and the Lower Jurassic deposits (photos from TNO, 2023).

Traditionally, very fine-grained rocks had been named with different terms such as “shales”, “claystones”, or “mudstones”. I will use the term “mudstone” and not “shale”, since the deposits have not suffered weathering (Lazar et al., 2015). I use the term “ironstone” to refer to the concretionary horizons (lateral extension unknown) and ironstone concretions when it is possible to identify the boundary.

The following classifications will be used for the sedimentary description of the deposits:

For the grain size classification I followed the approach from Trabucho-Alexandre et al., 2022 modified from Lazar et al., 2015, where it is established: “fine mudstones” as grain smaller than 10 µm, “medium mudstones” (fine and medium silt) from 10 to 30 µm, and “coarse mudstones” (coarser silt) from 30 to 62.5 µm. To indicate the size with the hand lens, Trabucho-Alexandre et al., 2022 used a different approach since the grains can be too small to be seen with naked eye. When fine mudstone dominates the fabric, the rock presents a soapy and soft texture to the touch. If the grain size is between 10 to 30 µm, the silt grains cannot be seen but the deposits have a rougher touch. When the grain size is between 30 and 62.5 µm the coarser silt grains can be seen using the hand lens.

To describe laminae and bed geometry I used the approach proposed by Campbell, 1967; it focuses on the thickness and genetics of the laminae and beds.

For the color classification, I used the Munsell Soil-Colour Charts (2009), by attributing a corresponding color name. In addition, color reflectance data was obtained using a Konica Minolta CM-700d handheld spectrophotometer at a 15 cm resolution between 1227.01 - 1313.9 mbs. I studied in detail the wavelengths (WL) of 550 nm (green) and 700 nm (red) including and excluding the ironstone values to study the main color shifts in the uppermost interval.

To establish bioturbation content I estimated the bioturbation index using the approach of Droser & Bottjer, 1986. Where lamination is still present and no bioturbation is observed: B.I. 1. If the primary lamination is present but there is some bioturbation: B.I. of 2 or 3. If the primary lamination is not visible, it could be due to a lower contrast between the grains or due to very high bioturbation that removed primary structures, B.I. 6, in this case, I will describe the deposits as massive.

3.3.2. Petrographic analysis

Twenty-five samples, representative of the deposit, were selected to produce thin sections (23 from the uppermost interval, 1 from the mid interval, and 1 from the lowermost interval) (Fig. 8) (Table 1).

The thin sections are 20 µm thick (ultra-thin sections) and polished by Wagner Petrographic, Utah, USA. They were analysed under a polarizing microscope in plane – (PLL) and cross-polarized (XPL) light.

The description was used to determine the primary characteristics of the deposits of the Lower Jurassic such as grain size, matrix cements, and (micro) fossil content. Subsequently, I established microfacies with the data obtained by using a similar approach as Ghadeer et al., 2011.

3.4. X-ray diffraction analysis (XRD)

The mineral composition was estimated by qualitative (13 samples) and semi-quantitative (25 samples) X-ray diffraction analysis (XRD). The samples selected were the same as for the petrological analysis (Table 1).

	Sample Code	Depth (mbsf)	Lithology
Upper Interval	MB1C	1283.15	Mudstone
	MB9C	1284.75	Mudstone
	MB13C	1285.55	Calcite nodule
	MB18C	1286.55	Mudstone
	MB26C	1288.15	Ironstone
	MB34C	1289.75	Mudstone
	MB36C	1290.15	Mudstone
	MB41C	1291.15	Mudstone
	MB47.2	1292.35	Ironstone
	MB52C	1293.25	Mudstone
	MB60C	1294.95	Mudstone
	MB69C	1296.75	Mudstone
	MB78C	1298.37	Mudstone
	MB87C	1300.3	Ironstone
	MB91C	1301.1	Mudstone
	MB97C	1302.28	Mudstone
	MB104C	1303.94	Calcite nodule
	MB115C	1306.19	Mudstone
	MB125C	1308.14	Ironstone
	MB132C	1309.60	Mudstone
	MB141C	1311.40	Mudstone
	MB146C	1312.40	Mudstone

	MB152C	1313.60	Mudstone
Mid Interval	MB158C	1511.50	Mudstone
Lower Interval	MB175C	1719.80	Mudstone

Table 1. Summary of the samples selected for the thin sections and the XRD analysis of the Lower Jurassic of the Molenbeersel borehole. Including the depth value and the main lithology of the sample.

The preparation of the samples for XRD included to McCrone mill the samples in 10 mL of ethanol for 12 minutes at 15000 rpm, using zirconium oxide grinding elements. The resulting slurry was air-dried overnight, disaggregated with a mortar and pestle, and backloaded into a sample holder with a cavity diameter of 25 mm. The samples run at the Department of Earth Sciences of Utrecht University on a Bruker D8 Advance with a LYNXEYE detector and a θ/θ goniometer.

I used a Cu-*K*α radiation (λ=1.54056 Å) and operate the tube at 40 kV and 40 mA. I used a 2.5° primary Soller slit, a fixed divergence slit (0.165 mm), and a motorized anti-scatter screen. Samples were measured from 3–80 °2θ, in 0.02° steps, and counted for 2 s per step, while rotating the samples at 0.25 Hz.

Afterward, for the quantitative analysis, 10 wt% of corundum was added to the sample powder, homogenized dry at the McCrone Mill for 1 minute at 15000 rpm, and backloaded for the second measurement.

For the semi-quantitative mineralogical study, I studied the relative % of each mineral found in comparison with the 10% corundum. The % were calculated by an estimation in comparison with the corundum added to each sample (10% of the weight). I focused on the mudstone's mineralogy.

3.5. Total Organic Carbon and sulfur data

The total organic carbon (TOC) and sulfur content were determined for 179 samples. Sample preparation took place at Utrecht University and subsequently, they were sent to Virginia Tech University (Benjamin Gill) for the C organic isotope, TOC and sulfur analysis.

Sample preparation involved powdering of the samples. Afterward, decalcify them in 3M HCl during 24h approximately. Rinse the samples by centrifuging three times at 3300 rpm for 15 minutes and dry them in an oven at temperatures lower than 60 °C. I homogenized the samples with an agate mortar and powdered them. They were placed in glass vials.

The TOC and sulfur data was studied including and excluding the ironstone samples in order to observe trends and links between these proxies and the presence of ironstones.

The two last samples from the lowermost interval (MB178 -179) were excluded from the graphs since the core was broken and the exact stratigraphic position of the samples is uncertain.

4. Results

4.1. Description of the Molenbeersel borehole

A total of ~ 36m of cores were described from the Triassic - Jurassic of the Molenbeersel borehole. Three intervals were recovered at different depths: uppermost interval (1283.15 - 1313.9 mbs); mid-interval (1510.1 - 1511.72 mbs) and, lowermost interval (1717.6 - 1720.37 mbs) (Fig. 8).

The general aspect of the deposit is rather homogenous. Dark grey argillaceous mudstones (> 50% of the grains smaller than 0.063mm) (clay and silt grain size) with ironstone horizons and concretions distributed throughout the core, and smaller carbonate concretions. Figure 9 shows an example of the Jurassic deposits recovered at the Molenbeersel borehole. The stratigraphic log of the Molenbeersel borehole is shown in Figure 10.

Fig. 9. Example of the general aspect of the Lower Jurassic of the Molenbeeersel borehole studied in this project between the depths of 1283.67 – 1288.72 mbs. (TNO, 2023).

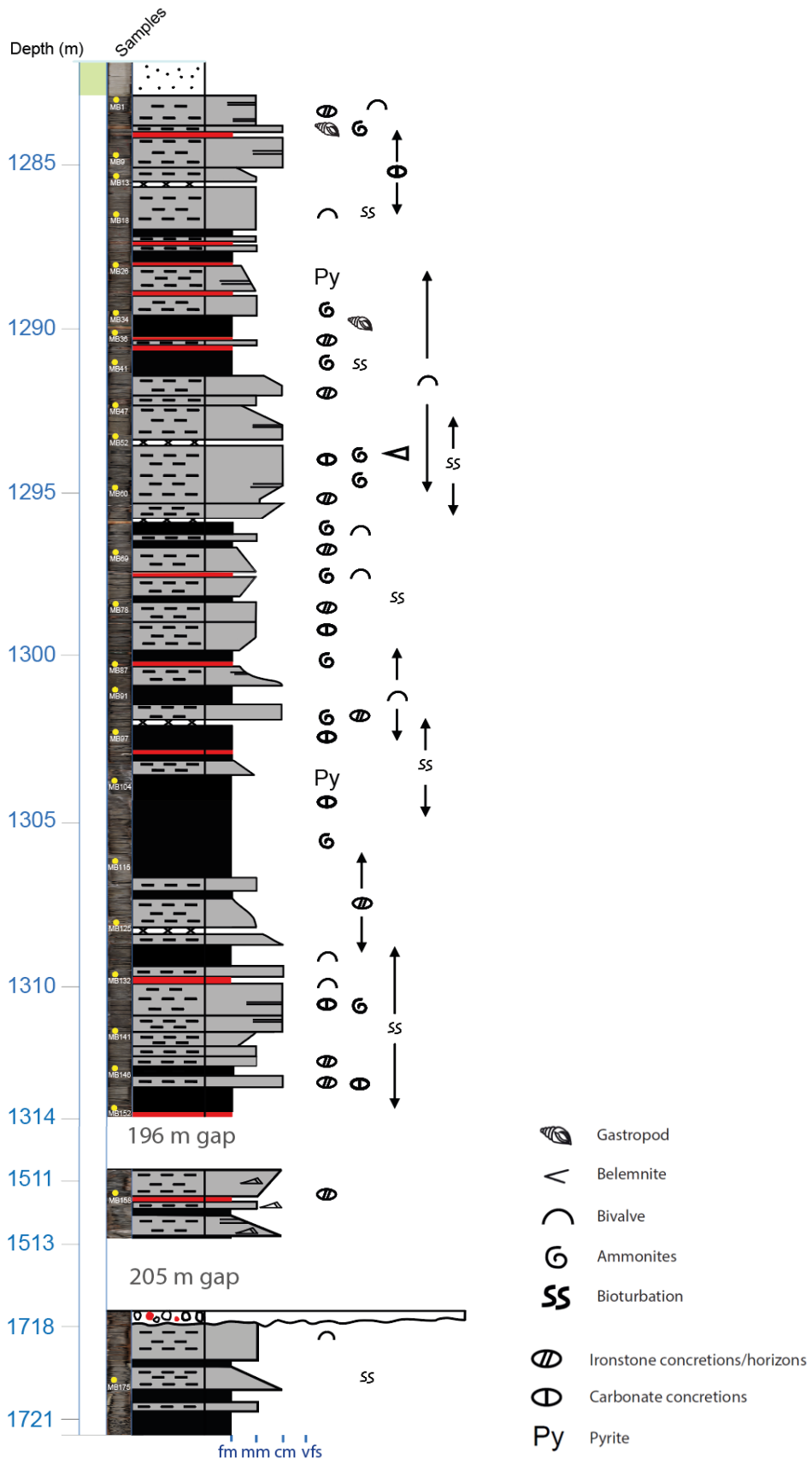
Depth (m)
Samples
1285
1290
1295
1300
1305
1310
1314
1511
1513
1718
1721
Py
Py
196 m gap
205 m gap
fm mm cm vfs
Gastropod
Belemnite
Bivalve
Ammonites
Bioturbation
Ironstone concretions/horizons
Carbonate concretions
Py
Pyrite

Fig. 10. Digitalized characterization (log) of the Lower Jurassic of the Molenbeersel borehole. We observe the three intervals and the depth gap between them. The deposits are composed of fine, medium, and coarse mudstones. Ironstones are present in the upper and mid interval. Ironstone and calcite nodules are present throughout the cores (except the lowermost interval). Macrofossil content is present, characterized by ammonites, gastropods, echinoderms, and bivalve bioclasts, they are found pyratized in some areas. Oxidized organic matter is also present. Grain size scale: fm, fine mudstone; mm, medium mudstone; cm, coarse mudstone.

Lamination was complicated to differentiate from the structures produced during the drilling process since the contrast between the grains from the deposits is not clear in some sections and the barrels were not cut in half

In the uppermost interval (1283.15 - 1313.9 mbs) spectrophotometry color analysis was performed. The red color is represented by the 700 nm wave length (WL), and the green color is represented by the 550 nm WL. The main 700 nm WL peaks represent the ironestones. To study the variations of color on the mudstones, a second curve was produced that explained the ironstone peaks.

Table 4 summarizes all the minerals identified in the XRD analysis.

Lowermost interval (1717.6 - 1720.37 mbs)

The lowermost interval is characterized by an alternation of medium and fine mudstone. The lower part is poorly preserved and the quality of preservation increases upwards. Lamination and bedding surfaces are not observed and displays a massive appearance. It presents a *medium dark gray (N4)* color that changes to *medium gray (N5)* at the mid and top part of this section. Some bioturbation (burrows of 1cm) and bioclasts can be distinguished in the middle part (Figure 12A). The uppermost part of this interval is characterized by a breccia, where mudstones and ironstone fragments can be found (Figure 11A). Ironstone horizons are not present in this interval. The XRD analysis is only conformed by one sample, which presented a very high percentage of pyrite. Quartz and clay minerals are present in lower values. It is thought to have analyzed a pyrite nodule, represented by group 3 in Figure 14C.

Mid-interval (1510.1 - 1511.72 mbs)

The mid-interval is characterized mainly by medium to coarse mudstone. From bottom to top, there is a decrease and a posterior increase in grain size. Starved ripples and horizontal lamination are present. Some ironstone horizons and concretions are also present in the middle part of the interval. This interval is characterized by a *medium dark gray (N4)* Munsell color that remains constant throughout the mid-interval. No bioturbation is present in this interval (B.I. 1). The XRD analysis studied one mudstone sample from this interval, the dominant mineral is quartz (relative 34%). Three families of clay minerals have been recognized (2:1 clay mineral with 14 Å *d* spacing, 2:1 clay mineral with 10 Å *d* spacing, and 2:1 clay mineral with 7 Å *d* spacing (probably kaolinite). Other minerals have been recognized in lower %: pyrite, chamosite, and albite. Forms part of the mineral group 1 showin in Figure 14A.

Uppermost interval (1283.15 - 1313.9 mbs)

At the bottommost part (1313.9 mbs), we observe an increase in grain size from fine mudstone to coarse mudstone (1310.9 mbs). If present, lamination is horizontal to semi-horizontal and thin to medium, not always continuous, and in the coarser-grained deposits. Presence of some coarser beds with a slight erosional surface and normal grading. The beds range from very thin to thin thickness. This part presents fluctuations in the bioturbation and fossil content: in the bottom part, lamination is not preserved (massive), followed by bedset with a B.I. 3, where primary lamination is still preserved (Fig. 12B). This lower interval presents low fossil content (mainly bivalves) and oxidized organic matter is common (Fig. 12C). There is a posterior decrease in grain size, which leads to a bedset of fine mudstone (from 1306 – 1303 mbs) with no lamination and conformed by very thin beds with ammonites, oxidized organic matter, and pyrite. This part of the deposits presents a *medium dark gray (N4)* color according to Munsell Soil-Colour Charts, 2009. In the spectrophotometry color analysis (Fig. 13), some small peaks in the red color (700 nm WL) can be observed throughout this part.

The middle part of this interval presents variations between fine, medium, and coarse mudstones, being the last grain size the dominating one. The lower and upper parts of this section present horizontal to semi-horizontal lamination, while the middle part is more massive. The bed thickness ranges from very thin to thin. In the lower section, bivalves and ammonites can be found, while in the middle-upper part, the bioturbation index increases up to 3, and more variation in fossil content is observed (bivalves, ammonites,

gastropods, and belemnites). Oxidized organic matter becomes common again during this part of the deposits. In the middle part of the deposits, we observe a higher variability in the color, between *N4*, *N5*, and *dark grey (N3).* In the spectrophotometry color analysis (Fig. 13), the lower part presents some smaller variations in the red color (700 nm WL); however, the upper part presents lower and more stable values.

The uppermost part of the core presents a general increase in grain size from fine and medium mudstone with pyrite (1290.5 – 1286 mbs) to medium and coarse mudstones (1286 – 1282 mbs). Most of this section presents horizontal to semi-horizontal lamination and the bed thickness shows higher variability ranging from very thin, thin, and medium thickness. Ironstones are present in this part (Fig. 11B). The contact between the Jurassic and the Cretaceous is an erosional surface with a clear change of color from dark grey to light beige (Fig. 11C); it presents a lower fossil content that comprises bivalves, ammonites, and gastropods. Oxidized organic matter is common in the upper-upper part of the deposits.

This part of the deposits presents a combination of colors *N3* and *N4* until the contact with the Cretaceous which in the spectrophotometry color analysis (Fig. 13), a higher variation in the red color (700 nm WL) is noticed that changes rapidly to lower and more steady values. The green (550 nm WL) does not present major fluctuations in the curve where the ironstones are not represented (Fig. 12).

The XRD analysis studied 23 samples, which can be subdivided into two groups: Group 1 (Fig. 14A), the dominant mineral is quartz (relative 34%). Three families of clay minerals have been recognized (2:1 clay mineral with 14 Å *d* spacing, 2:1 clay mineral with 10 Å *d* spacing, and 2:1 clay mineral with 7 Å *d* spacing (probably kaolinite). Other minerals have been recognized in lower %: pyrite, chamosite, and albite. Moreover, Group 2 (Fig. 14B), where the dominant mineral of the ironstones is siderite (~ 66%). Quartz, calcite, and clay minerals (kaolinite) are also present.

Figure 15 shows the relative mineral changes throughout the core for the mineral Group 1. In the lower part of this interval, the quartz, the clay minerals and the pyrite to a lesser extent, display the same trend until the middle part. Afterwards, the trend between the quartz and the rest of the minerals diverges and becomes inverted until the upper part of the interval.

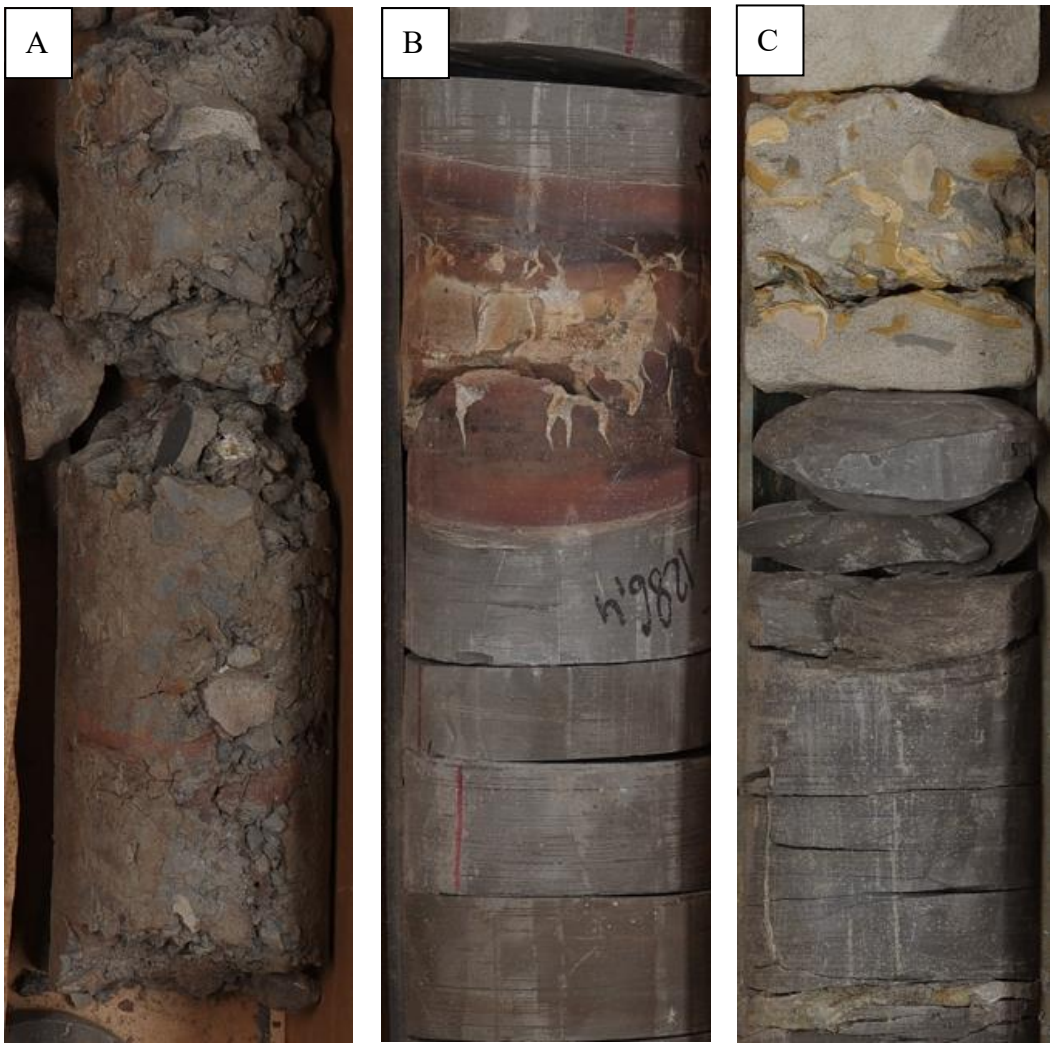

Fig. 11. The deposits of the Lower Jurassic of the Molenbeersel borehole. **A)** Breccia located at the top of the lowermost interval where mudstone and ironstone clasts can be observed between the depths of 1717.63 - 1717.40 mbs. **B)** Example of the deposits of the uppermost interval: septarian ironstone and mudstones between the depths of 1287.61 - 1287.44 mbs. We observe that the boundaries of the ironstone is well observed. **C)** Contact between the Cretaceous (lighter color) and the Lower Jurassic (darker color) at a depth of 1283.12 mbs

Fig. 12. Example of the fossil and bioturbation content of the Lower Jurassic in the Molenbeersel borehole. **A)** Example of a burrow (white arrow) in the lowermost interval of the core at 1718.84 mbs. The burrow presents pyritization in the interior part of the bioturbation. **B)** Example of a pyritized bioturbation (white arrow) at 1310.64 mbs**. C)** Example of oxidized organic matter (white arrow) at 1313.7 mbs.

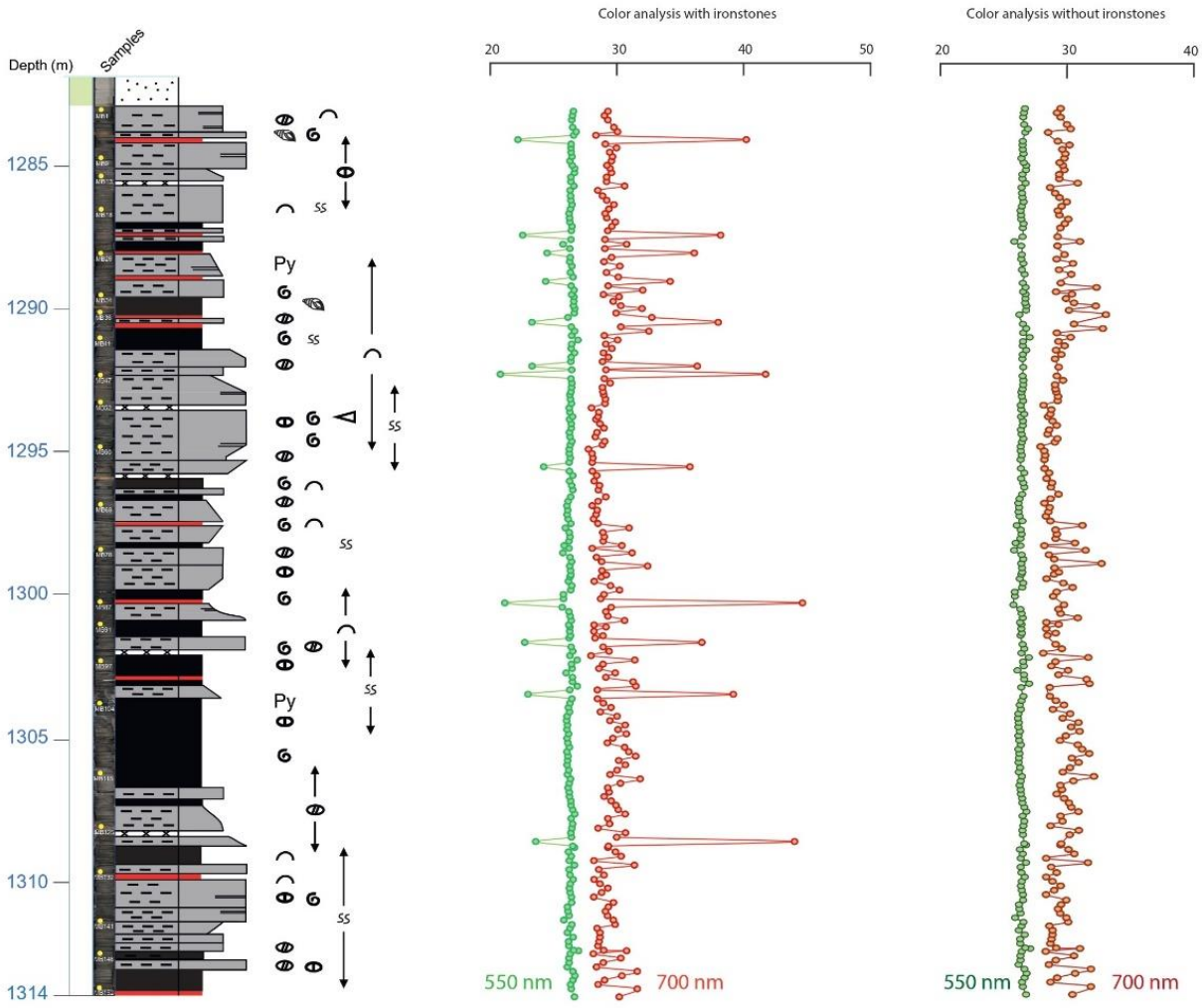

Fig. 13. Color analysis of the Molenbeersel borehole with the red (700WL) and green (550WL) color data. In the curve including ironstones (middle), we observe that the main peaks (higher for the 700WL; lower for the 550WL) correspond to the ironstone horizons and concretions. When removing the peaks, the curves present a more homogenized trend. The 550WL green does not present important shifts. The 700WL red curve presents minor changes and an interval of lower values without smaller shifts between 1291 – 1280 mbs.

Sample code	Depth	Group	Quartz	Calcite	Clay mineral 14A	Clay mineral 10A	Clay mineral 7A	Chamosite	Albite	Pyrite	Siderite
MB1C	1283.15	1	x		x	x	x	x	x	x	
MB9C	1284.75	1	x		x	x	x	x	x	x	
MB13C	1285.55	1	x		x	x	x	x	x	x	
MB18C	1286.55	1	x		x	x	x	x	x	x	
MB26C	1288.15	2	x	x		x	x				x
MB34C	1289.75	1	x		x	x	x	x	x	x	
MB36C	1290.15	1	x		x	x	x	x	x	x	
MB41C	1291.15	1	x		x	x	x	x	x	x	
MB47C	1292.35	1	x		x	x	x	x	x	x	
MB52C	1293.25	1	x		x	x	x	x	x	x	
MB60C	1294.95	1	x		x	x	x	x	x	x	
MB69C	1296.75	1	x		x	x	x	x	x	x	
MB78C	1298.37	1	x		x	x	x	x	x	x	
MB87C	1300.3	2	x	x		x	x				x
MB91C	1301.1	1	x		x	x	x	x	x	x	
MB97C	1302.28	1	x		x	x	x	x	x	x	
MB104C	1303.94	1	x		x	x	x	x	x	x	
MB115C	1306.19	1	x		x	x	x	x	x	x	
MB125C	1308.14	2	x	x		x	x				x
MB132C	1309.60	1	x		x	x	x	x	x	x	
MB141C	1311.40	1	x		x	x	x	x	x	x	
MB146C	1312.40	1	x		x	x	x	x	x	x	
MB152C	1313.60	1	x		x	x	x	x	x	x	
MB158C	1511.50	1	x		x	x	x	x	x	x	
MB175C	1719.80	3	x				x			x	

Table 2. All minerals identified in XRD analysis gathered in three groups.

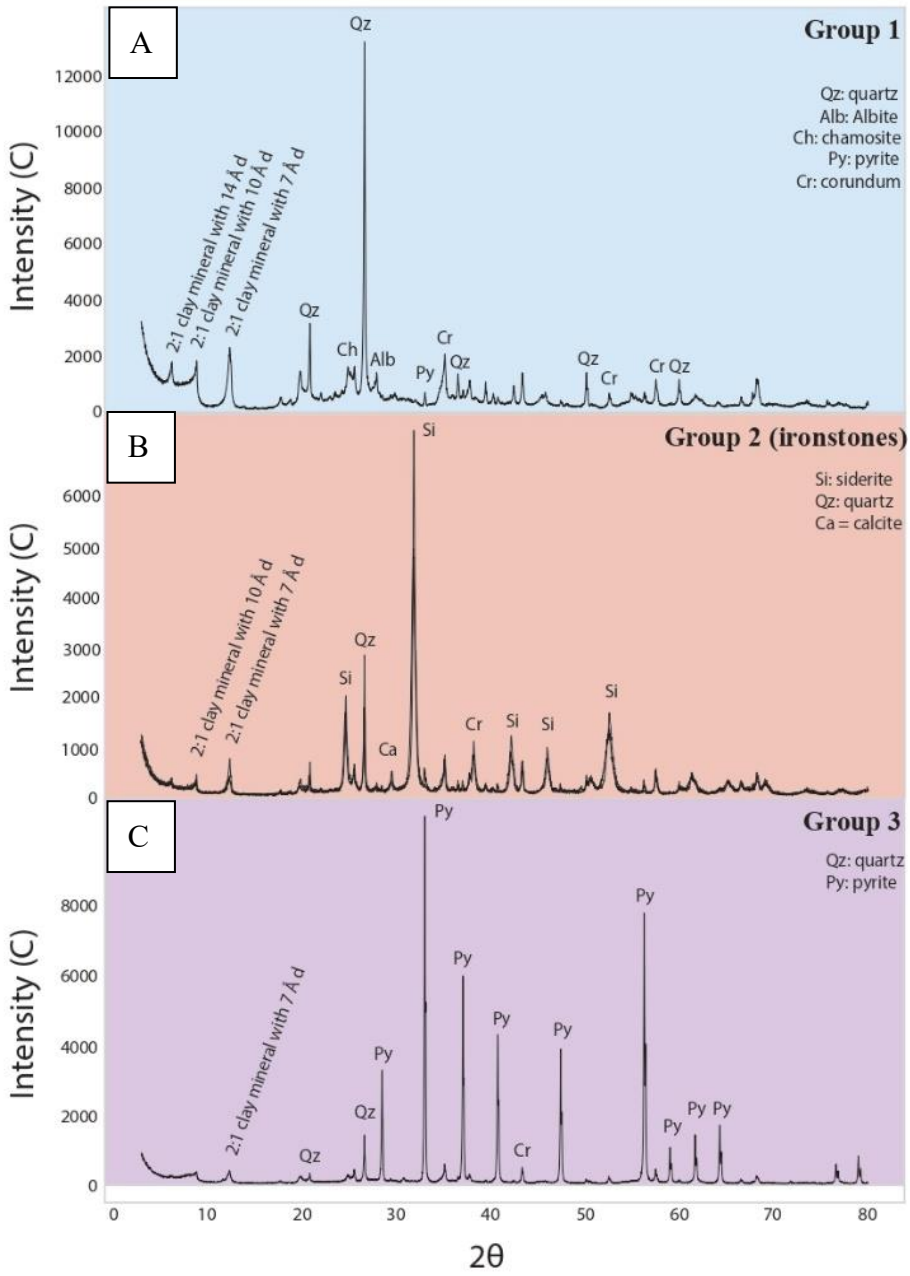

Fig. 14. XRD results of the different deposits from the Molenbeerel core. **A)** Represents the XRD results of Group 1, which includes all the mudstone samples of the upper and middle interval (1227.01 - 1511.72 mbs). The main minerals identified are quartz, clay minerals (14, 10, and 7 Å spacing), chamosite, pyrite, and albite. **B)** Represents the XRD results of Group 2, which includes the ironstones from the uppermost interval. The ironstones are composed mainly of siderite, quartz, calcite, and clay minerals (10 and 7 Å spacing). **C)** Represents the XRD results of Group 3, which includes the one sample analyzed from the lowermost interval. The main minerals are pyrite, quartz, and kaolinite (7 Å spacing clay mineral).

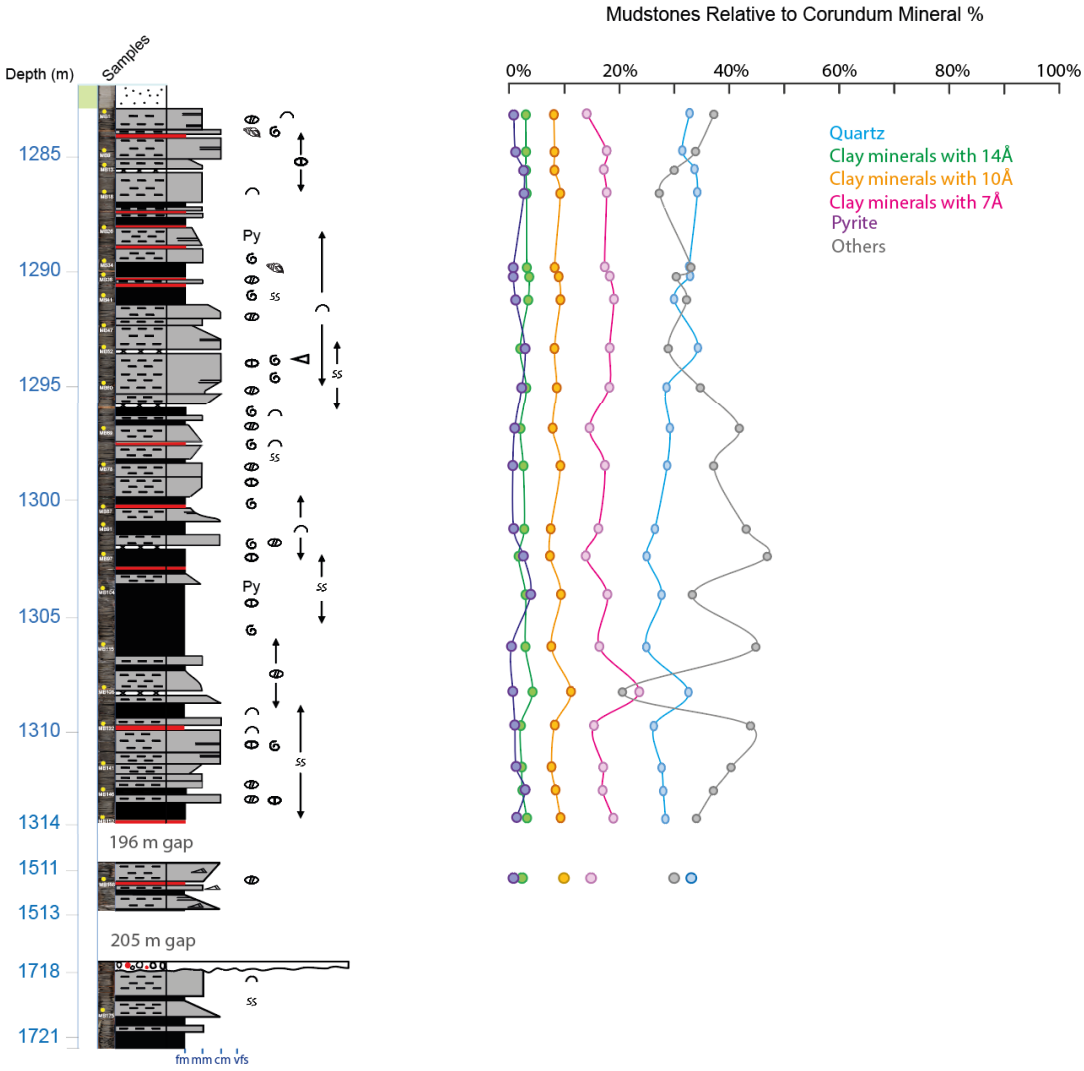

Fig. 15. Relative mineral changes (%) throughout the core. The main minerals identified have been plotted to observe general trends throughout the core. The quartz is the dominant mineral for the mudstones in all the samples. The trend of the quartz and the kaolinite (7 Å *d* spacing clay mineral) and the 10 Å *d* spacing clay mineral, present very similar tendencies in the lower part of the uppermost interval of the core (1283.15 - 1313.9 mbs). The trend of the clay minerals remains the same in the upper part, but the quartz content presents more variations. The pyrite content slightly shifts but remains rather low throughout the core.

4.2. Facies analysis

4.2.1. Lithofacies

Two main mudstone lithofacies types are identified based mainly on the grain size of the deposits since sedimentary structures are scarce and fossil content is not representative enough (Table 3). 1) Fine-grained mudstone, 2) Medium to coarse-grained mudstone.

Code	Lithofacies
LF1	Fine-grained mudstone
LF2	Medium to coarse-grained mudstone

Table 3. Overview of the lithofacies

Fine-grained mudstone (LF1)

The lithofacies LF1 consists of dark grey fine-grained mudstones (clay and very fine-silt grain size) (Fig. 16A, 16B). When lamination is visible, it presents sub-horizontal to horizontal and discontinuous geometry. Ammonites, bivalve shells, and gastropods are found in this lithofacies (Fig. 16C**)**. Iron and carbonate concretions can be present in different forms (rounded to elongated), usually with a few centimeters in size for the longest axis (1-5 cm). If present, bioturbation is found as burrows with a diameter ranging from 0.3 to 1 cm and sometimes with pyritized filling**.**

Medium to coarse-grained mudstone (LF2)

The lithofacies LF2 is characterized by dark and medium grey mudstones (Fig. 16D**)**. The grain size ranges from medium to coarse mud (fine, medium, and coarse silt). Lamination is present in some areas with sub-horizontal to horizontal, continuous, and parallel geometries. Very thin to thin bed surfaces can be found with a normal grading trend. Regarding the fossil content, it presents bioclasts (mainly shell fragments), ammonites, belemnites, gastropods, and oxidized organic matter (Fig. 16D). Bioturbation can be present.

Ironstone and carbonate concretions are common with different thicknesses and geometries ranging from rounded to elongated, and between a few cm to

decimeters (Fig. 16E). Some of the ironstones present septarian calcite veins (Fig. 16F).

Ironstones

Ironstones are not established as a lithofacies, but a short description is added due to their abundance in the deposits. Ironstones can be found with two main geometries**:**

- Small ironstone concretions: Small rounded to elongated concretions ranging in size between 0.5 – 2 cm (diameter). Red color and sometimes, red discoloration around them in the mudstone (Fig. 16E).
- Ironstone horizons and big ironstone concretions: they present a red color. The size of the horizons/concretions is bigger than the barrels and the limits of them are not identifiable. Some of them display septarian calcite veins (Fig. 16F).

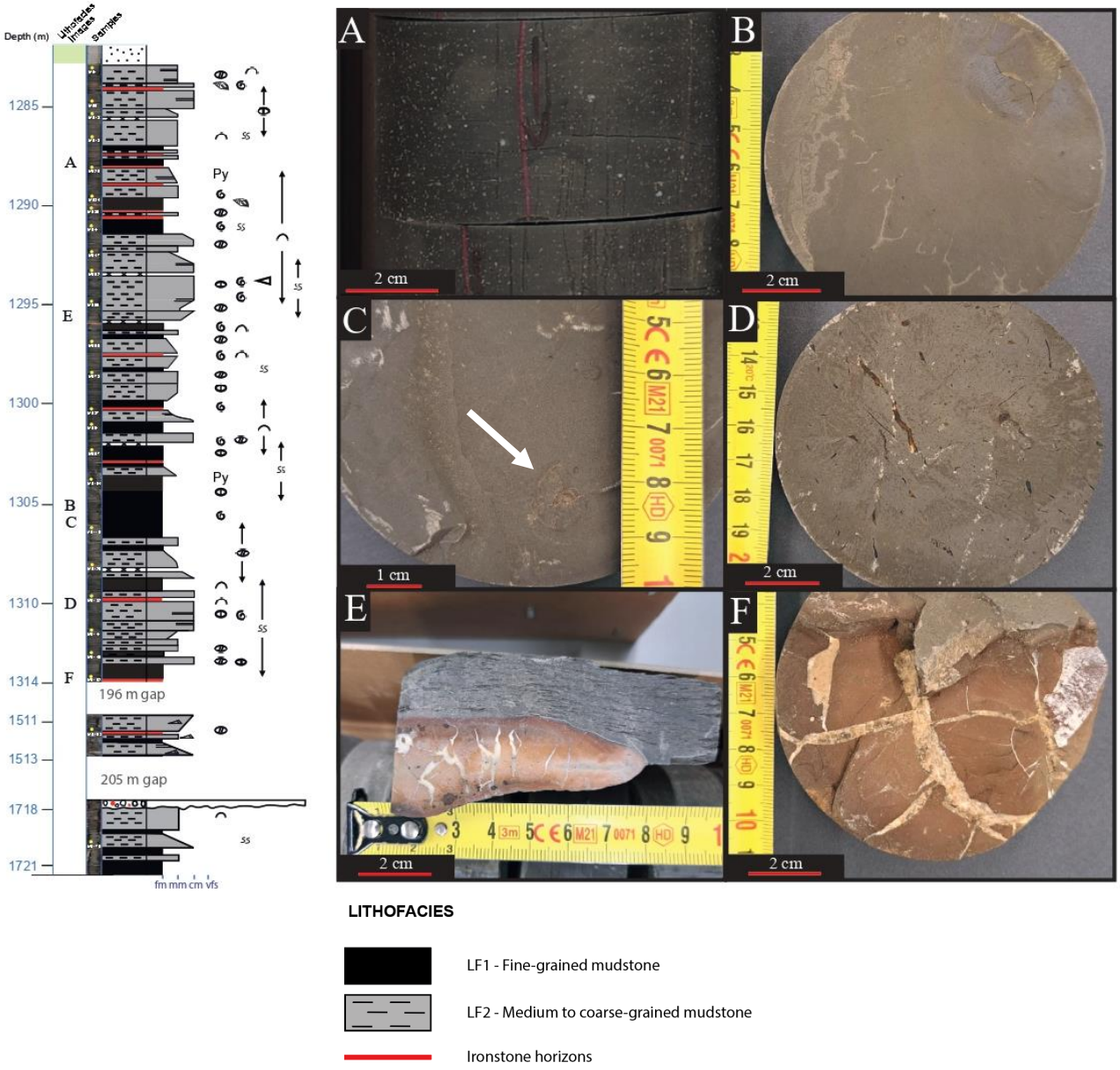

Fig. 16. Lithofacies characterization of the Molenbeersel borehole. **A)** Example of lithofacies 1 (LF1) with massive appearance (1288.70 mbs). **B)** Example of LF1 from above with very fine mudstone and no fossil or bioturbation content (1305.3 mbs). **C)** Example of LF1 with an ammonite fossil marked with a white arrow (1305.70 mbs). **D)** Example of lithofacies 2 (LF2), with coarser grain size (1310.62 mbsf). Oxidized organic matter is also present in this sample. **E)** Example of LF2 where the primary lamination has been deformed due to the growth of the ironstone nodule with internal calcite veins (1296.68 mbsf). **F)** Example of septarian ironstone (1313.9 mbsf). Legend: Black: LF1; Grey: LF2. Grain size scale: fm, fine mudstone; mm, medium mudstone; cm, coarse mudstone.

4.2.2. Microfacies

Six microfacies are established focusing mainly on the primary features of the deposits such as grain size, primary structures, and fossil content (Table 4). In Figure 17**,** the microfacies are indicated for each sample next to the digitalized log.

Code	**Microfacies**
MF1	Massive to slightly laminated fine mudstone
MF2	Fine to medium mudstone, with lamination and bed surfaces
MF3	Fine mudstone with bioclasts
MF4	Massive to laminated, medium to coarse mudstones
MF5	Medium to coarse mudstone, with lamination and bedding surfaces
MF6	Ironstones

Table 4. Overview of the microfacies

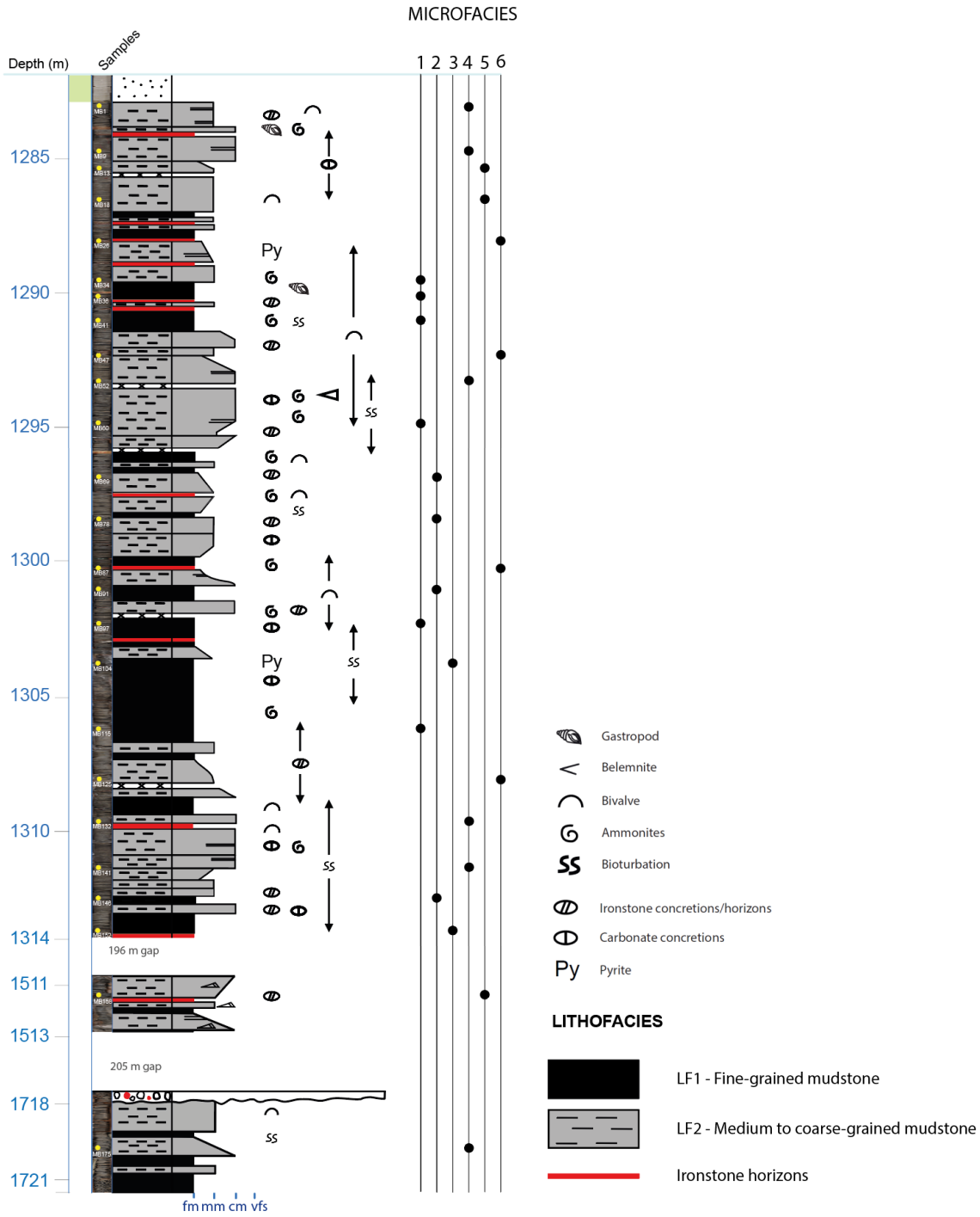

Fig. 17. Microfacies location in the Lower Jurassic of the Molenbeersel borehole next to the log. Microfacies 1: massive to slightly laminated fine mudstone. Microfacies 2: Fine to medium mudstone, with lamination and bed surfaces. Microfacies 3: Bioclastic fine mudstone. Microfacies 4: Massive to laminated, medium to coarse mudstones. Microfacies 5: Medium to coarse mudstone, with lamination and bedding surfaces. Microfacies 6: Ironstones.

MF1: Massive to slightly laminated fine mudstone

Microfacies 1 (MF1) consist of fine mudstones, massive or with discontinuous lamination (Fig. 18A). The fine-grained fraction represents more than 90% of the rocks. It is composed mainly of quartz, clay minerals**,** muscovite, bioclast fragments, and (amorphous) organic matter.

Some bigger clasts can be found in a ratio of 3 – 6 %, they are formed by disarticulated bioclast debris, rounded lithoclasts of polycrystalline quartz, clay lithoclasts, and diagenetic pyrite. The isolated articulated or disarticulated bioclasts present a size that ranges from 200 to 1800 µm. The main types of fossils are echinoderms and bivalve shells. Pyrite (~ 4%) is also found in aggregates (~ 1000 µm) (Fig. 18A) or isolated with framboidal and euhedral habits (~ 90 µm size)**.**

Where preserved, lamina geometries vary from even or wavy, nonparallel to parallel, and discontinuous. Very thin laminae can be distinguished by a higher accumulation of grains, such as clay minerals, quartz, or small bioclast debris, with very low lateral extension. Where no lamination is observed, a massive appearance.

MF2: Fine to medium mudstone, with lamination and bed surfaces

Microfacies 2 (MF2) is characterized by fine to medium mudstone. The coarser fraction consists mainly of bioclasts and diagenetic pyrite, with an average size of 800 µm. The finer fraction (> 90%) of the microfacies is composed of clay minerals, quartz, bioclast fragments, muscovite, and organic matter.

The fossil content is low (< 3%) and bioclasts are found as broken fragments with angular edges (size ranges from 400 to 3000 µm). Echinoderms and shells are present. Bioclasts can be found isolated or accumulated in bed surfaces. Diagenetic pyrite is also found in aggregates (~ 600 µm) or isolated with framboidal and euhedral habits (80 µm) (Fig. 19F). In some samples, mud lithoclasts are present with an average size of 600 µm.

This microfacies presents a laminated internal structure. Lamina size ranges from very thin to thin lamina. They present an even and discontinuous geometry. Lamina can be horizontal and/or small-scale cross-lamination. In

some cases, the pyrite crystals follow the geometry of the primary lamination (Fig. 19D). The bedding planes are identifiable due to the accumulation of grains. Broken bioclasts, quartz grains, and moscovite are present in discontinuous lags (~ 90 μm = very fine sand grain size) at bed bases (erosional surfaces) (Fig. 18B).

MF3: Fine mudstone with bioclasts

Microfacies 3 (MF3) consists of fine mudstone with larger bioclasts, fossils, and bioturbation (Fig. 18C). The coarse-grained components consist of bioclasts (~ 10%) and diagenetic pyrite (~ 5%). The finer fraction of the rocks is composed mainly of quartz, clay minerals, muscovite, and organic matter.

MF3 presents larger bioclasts (from 200 to 3000 μm), broken and unbroken. Ammonites, echinoderms, gastropods, and shells of bivalves can be distinguished (Fig. 19E). Bioturbation is also present as burrows filled with fecal pellets, the cement between the pellets has a calcite composition, which indicates early cementation since the primary geometry of the pellets is not modified (Fig. 18C). The fossils can be found dispersed in the rock, without being in contact with each other, and with no specific orientation. In some cases, the original composition of the bioclast has experienced mineral replacement by chalcedony, losing the original internal structure. In other samples, pyrite has grown inside the bioclasts maintaining the original structure. Both framboidal (~ 41 μm) and aggregates (~ 700 μm) of pyrite are visible.

Where lamina is visible, it presents an even and discontinuous geometry. Lamination can be horizontal or small-scale cross-lamination. In some cases, the pyrite crystals follow the geometry of the primary lamination. The laminae are usually visible due to the contrast between the different grain types such as quarts, bioclast fragments, or clay minerals. No bedding is observed.

MF4: Massive to laminated, medium to coarse mudstones

Microfacies 4 (MF4) is characterized by medium to coarse mudstones (Fig. 18D). The coarser fraction consists of quartz grains (monocrystalline), mudstone clasts, diagenetic pyrite, and bioclasts fragments. The matrix of the

rocks is composed mainly of clay minerals**,** quartz, muscovite, bioclast debris, and organic matter.

Bioclast fragments (< 3%) and fossils can be found with a size ranging from 200 to 2000 µm. Echinoderms, ammonites, gastropods, and bivalve shells mainly (Fig. 19A). Some of the bioclasts have been replaced by chalcedony losing the original internal structure. In addition, mud lithoclasts are present in some of the samples (~ 500 µm). Pyrite (~ 4%) is present as dispersed framboids (~ 90 µm) and bigger aggregates (~ 1300 µm) compared to the other microfacies.

This microfacies can present lamination. The lamination ranges from very thin, even to wavy, horizontal, and discontinuous. The internal structure is visible due to a higher accumulation of grains and contrast (clay minerals, quartz grains, bioclasts…), with a small lateral extension. Where the lamination is not observed, a massive appearance is observed. There is no evidence of bed surfaces.

MF5: Medium to coarse mudstone, with lamination and bedding surfaces

Microfacies 5 (MF5) is characterized by medium to coarse–mudstones. The coarser grains consist of bioclasts, quartz, and diagenetic pyrite. The matrix of the rocks is composed of clay minerals, muscovite, quartz, bioclast fragments, and organic matter (Fig. 19B).

Skeletal bioclast content is rare (~ 1%) compared to the other microfacies, with an average size of 500 µm. Big lithoclasts of polycrystalline quartz can be present (~ 750 µm), they could also be fossils where the mineral replacement took place, however, the shape of the grain is not clear. Both framboidal (~ 50 µm) and big aggregates (~ 1000 µm) of pyrite are visible. Around the big pyrite aggregates, we can observe calcite cement veins.

Laminae geometry varies from very thin to thin thickness, continuous to discontinuous, and horizontal to small-scale cross-lamination. In some cases, the pyrite crystals follow the geometry of the primary lamination. Lamination is usually visible due to the accumulation of grains such as quarts, bioclast fragments, or clay minerals. Bed surfaces can be observed, presenting a bioclast, muscovite, and quartz lag; and a fining upwards trend (normal grading) of the grain size (Fig. 18E, F). Bed surfaces can be continuous or discontinuous. In some areas, laminae pinch out in the bed surfaces.

MF6: Ironstones

Microfacies 6 (MF6) represents the ironstones from the Jurassic deposits. They are found in two forms: 1) very fine mudstones with articulated bioclasts (Fig. 19C); 2) crystalline texture with calcite veins (septarian veins).

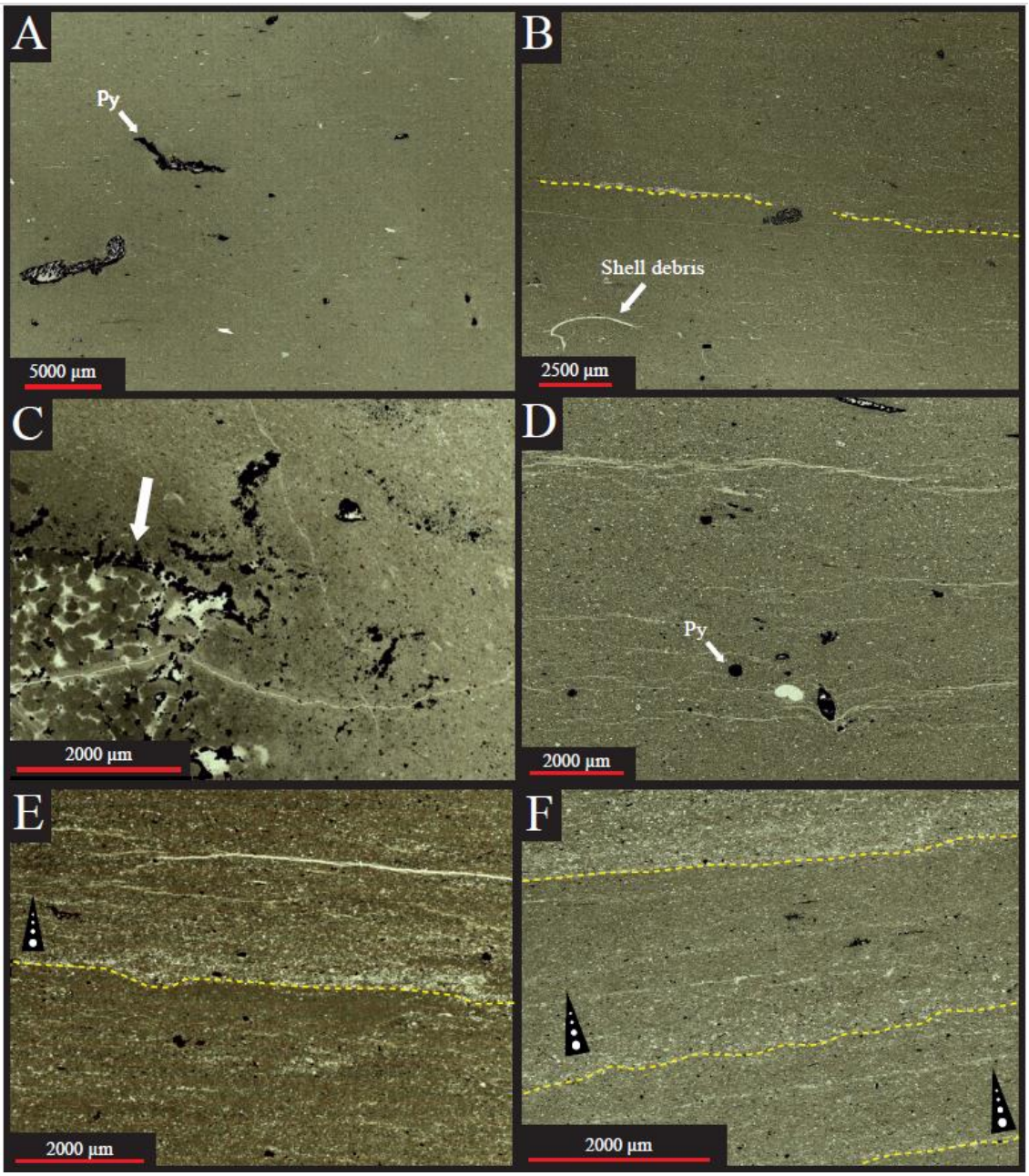

Fig. 18. Plane-polarized-light optical micrographs of the Lower Jurassic in the Molenbeersel borehole and microfacies characterization**. A)** Example of MF1 with a massive appearance in fine-mudstones (MB41, 1291.15 mbs). Py: pyrite. **B)** Example of MF2, erosive bed surface with detrital quartz and bioclast silt-size grains lag (yellow dashed lines) and bioclasts (MB69, 1296.75 mbs). **C)** Example of MF3, burrow with fecal pellet accumulation and

calcite cement, indicating early cementation (white arrow) (MB102, 1303.94 mbs). **D)** Example of MF4, coarser grain size compared to the prior microfacies can be observed with a discontinuous lamination. Pyrite (Py, arrow) in larger aggregates and framoidal and ehuedral forms (MB52, 1293.25 mbs). **E)** Example of MF5 with an erosive bed surface with an accumulation of quartz and biolcast detrital grains lag (yellow dashed line). Normal grading can be observed (Symbol) (MB18, 1286.55 mbs). **F)** Example of MF5 where three bed surfaces can be observed (dashes yellow lines); the lower and middle planes present a normal grading trend (Symbol). The uppermost bed plane presents a change to coarser grain size (MB26, 1288.15 mbs).

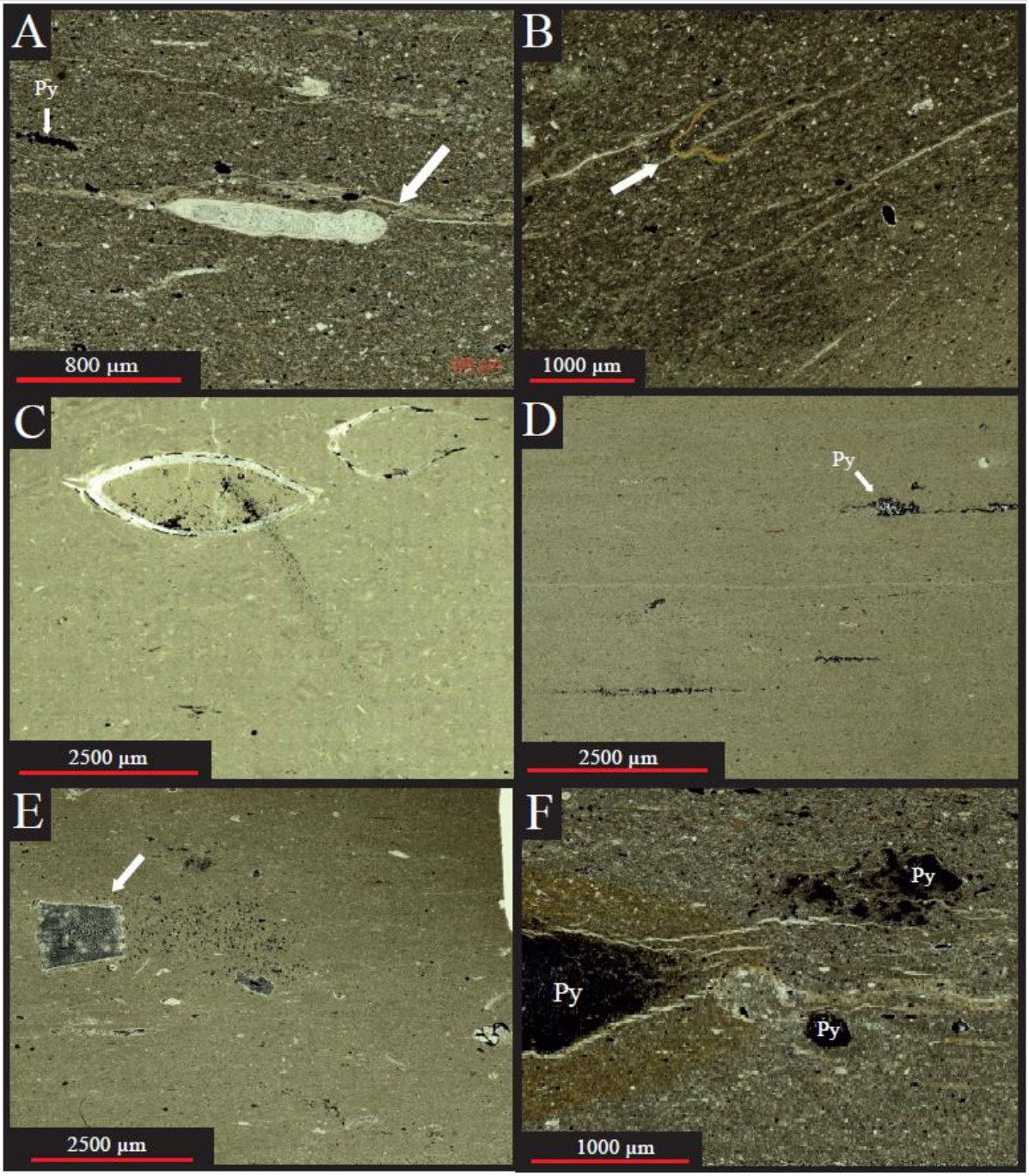

Fig. 19. Plane-polarized-light optical micrographs of the Lower Jurassic in the Molenbeersel borehole. **A)** Example of an ammonite bioclast (white arrow), pyrite (Py), and quartz silt size grains from MF4 (MB9, 1285.75 mbs). **B)** Example of organic matter with an orange color (white arrow) (MB13, 1285.55 mbs). The unflattened shape indicates early cementation. **C)** Example of an ironstone concretion with a very fine grain size that contains articulated bivalve shells from MF6 (Mb26, 1288.15 mbs). **D)** Example of horizontal lamination where authigenic pyrite framboidal grains (Py) follow the primary lamination in MF1 (MB115, 1306.19 mbs). **E)** Example of echinoderms (white arrow) and gastropod from MB3 (MB152, 1313.60 mbs). **F)** Example of pyrite aggregate (Py) and veins from MF4 (MB9, 1285.75 mbs).

4.4. Total Organic Carbon (TOC), sulfur and carbon isotope record

Here, I present the first $\delta^{13}C_{org}$, Total Organic Carbon (TOC) and sulfur record obtained from the Molenbeersel borehole. The data includes the three intervals.

The organic carbon isotopes ($\delta^{13}C_{org}$) present an average value of ~ 24.5‰ (VPDB) (Fig. 20, green curve). The lowermost interval (1717.6 - 1720.37 mbs) presents very anomalous values, ranging between -30.0‰ and -5.0‰, this chaotic trend may indicate some problem during the measuring of the $\delta^{13}C_{org}$. The middle interval (1510.1 - 1511.72 mbs), presents some variability but in a smaller scale, between with an average value of -23.1‰ (Fig. 20, green). The uppermost interval presents intervals of higher fluctuations and intervals of more homogeneous values. Between the base and 1307 mbs the values present more oscillations; between 1307 – 1301 mbs, the values present a more steady trend. Between the depths of 1301 – 1292 mbs, the values present high variability again. Finally, the values present a more homogeneous trend with little flyers from the depth of 1292 mbs until the top (Fig. 20, green).

When comparing the values to the lithology, it seems that there is a correlation between the grain size and the presence of flyers (anomalous values). In the two intervals where the $\delta^{13}C_{org}$ curve presents more fluctuations, a general increase in the grain size of the deposits can be observed (medium to coarse mudstone). The intervals with more homogeneous values can be correlated with the intervals with higher content of fine mudstone deposits.

The TOC values present a rather homogeneous trend with some isolated positive flyers. The mudstones present an average value of 1.3 wt%. Two types of anomalies can be observed in Figure 20 (dark blue), in the uppermost

interval (1283.15 - 1313.9 mbs) small positive anomalies are found in the middle and upper part of this interval, representing the ironstones, with an average TOC value of 2.8 wt%. The second important TOC anomaly is observed between the depths of 1717.80 and 1718.20 mbs (located in the lowermost interval), reaching values of 8.24 wt%. In this part of the core, no ironstones have been described; therefore, the shift are influenced by other factors. For a better study of the TOC in the mudstones, the ironstone data points have been removed to observe trends in the mudstone deposits (Fig. 20, light blue). My observations will focus on the uppermost interval: a gradual shift can be observed displaying a gradual increase around the 1305 mbs, followed by a posterior decrease until 1295 mbs and an increase until 1287 mbf. The uppermost part presents a decreasing trend. However, the data is rather homogeneous.

The sulfur data presents a more heterogeneous trend (Fig. 20, orange). A positive sulfur anomaly can be observed in the lowermost interval, from 1717.6 to 1719.6 mbs, with values reaching up to 7.5 wt%. Some ironstones present higher sulfur values (between 5 and 8 wt%). When removing the ironstone values (Fig. 20, pink), the heterogeneous trend remains in comparison to the TOC data without ironstones, most of the high peaks and shifts remain in the curve, presenting an average sulfur value of 1.21 wt%.

When comparing the $\delta^{13}C_{org}$, TOC and sulfur data, we observe different trends. While some of the TOC and sulfur high-peaks match due to the presence of ironstones, some of the sulfur peaks are described in areas of lower TOC values. According to the TOC – sulfur shift in the lowermost interval, we observe that in the sulfur curve the shift starts before the TOC positive excursion and drops to lower values at the same depth. The $\delta^{13}C_{org}$ is not fully reliable for the lowermost interval, but important fluctuations are observed, indicating the probability of a complex interval. There is a higher variation in the data of sulfur and $\delta^{13}C_{org}$ throughout the deposits. Figure 21 studies the correlation coefficient (R^2) between the TOC and sulfur data. It presents an irrelevant correlation ($R^2 = 0.123$), indicating a non-linear relationship between both variables. As we can observe, the ironstones present a high range of sulfur values but similar TOC values, similar to what can be observed for the mudstones of the uppermost interval (with lower TOC values). The mid-interval presents similar values of TOC and some variation in sulfur, but compared to the uppermost interval the values are more homogenized. The lowermost interval presents the highest variability represented by either high TOC – high sulfur data points or; low TOC – and variable sulfur values.

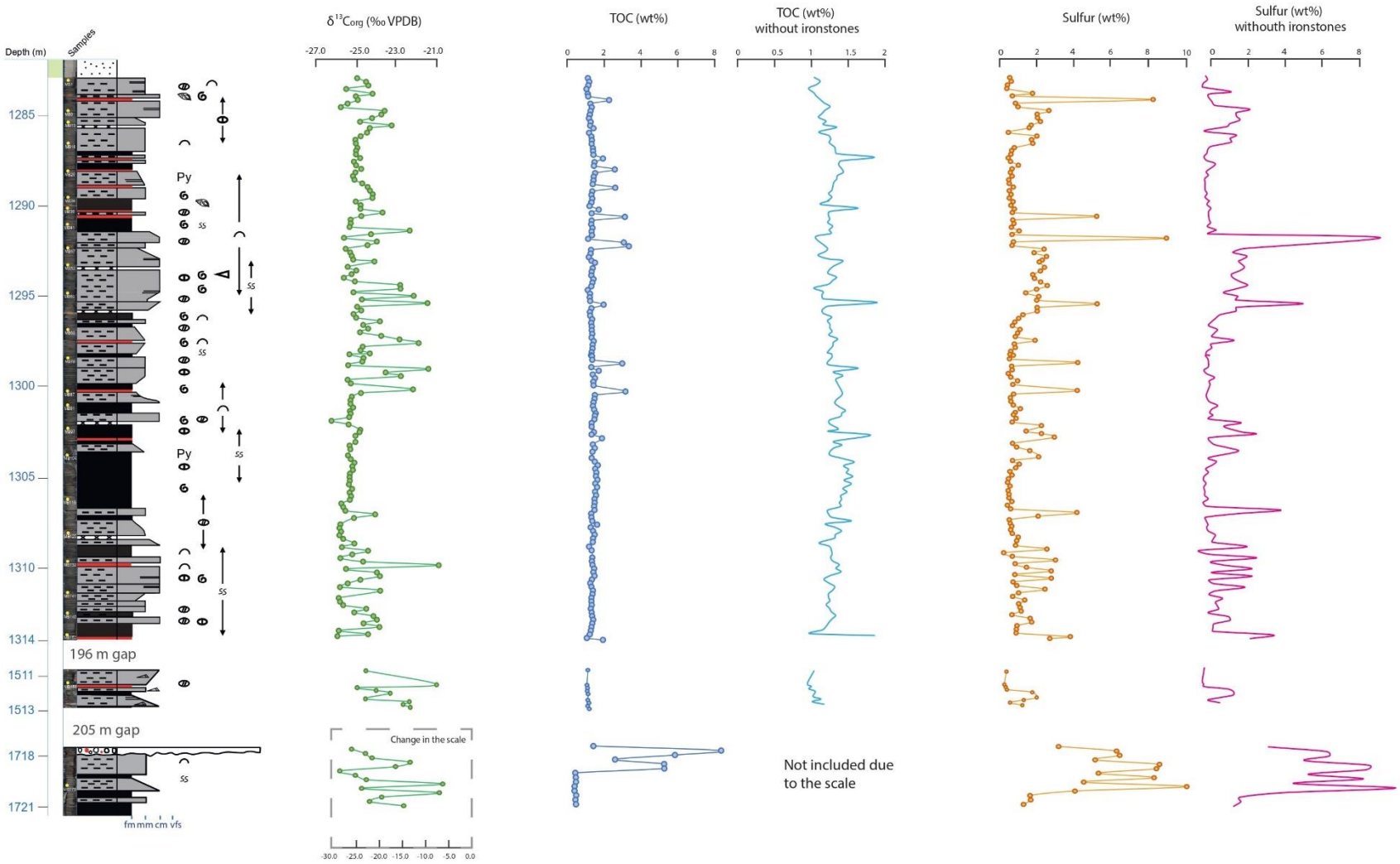

Fig. 20. $\delta^{13}C_{org}$, TOC and Sulfur record of the Lower Jurassic of the Molenbeersel borehole. The figure presents five curves. Green: $\delta^{13}C_{org}$ complete, where the data presents rather stable values with the exception of the lowermost interval. Dark blue: TOC data complete, where two positive anomalies can be observed: 1) upper interval due to the presence of ironstones; 2) in the lowermost interval where ironstones are not present. Light blue: TOC data without the ironstone peaks. More shifts can be distinguished but still, a rather stable trend can be observed. Orange: Sulfur data complete, higher heterogeneity is observed in all three intervals. Pink: Sulfur data without the ironstone values. Heterogeneous trend, many of the positive peaks remain after removing the ironstone peaks. A major shift is present in the lowermost interval, but reaching deeper depths than the TOC excursion.

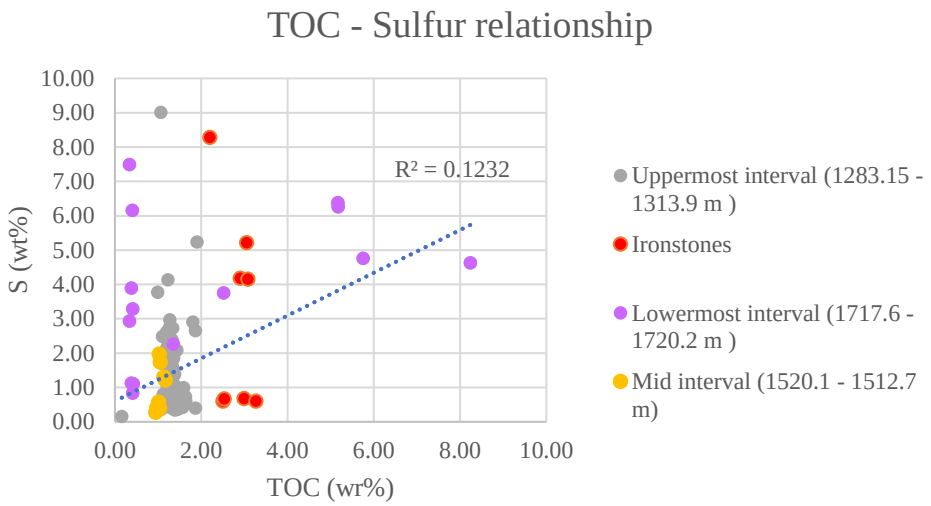

Fig. 21. Relationship between the TOC and sulfur data of the deposits of the Lowe Jurassic of the Molenbeersel borehole. The R^2-value that provides information about the correlation between both variables presents a lower association, indicating a non-linear relationship between the TOC-sulfur data. The record has been grouped into four groups: grey-uppermost interval, yellow-mid interval, pink-lowermost interval, and red, ironstones. As we can observe, the ironstones present a high range of sulfur values but similar TOC values, similar to what can be observed for the mudstones of the uppermost interval (with lower TOC values). The mid-interval presents similar values of TOC and some variation in sulfur, but compared to the uppermost interval the values are more homogenized. The lowermost interval presents the highest variability represented by either high TOC – high sulfur data points or; low TOC – and variable sulfur values.

5. Discussion

5.1. Lithostratigraphy of the Molenbeersel borehole

In this project, I studied the deposits of the Molenbeersel borehole. In total, 36 m of core were recovered from approximately 500 m of the Lower Jurassic (Edwin Maes, 1990). The recovered rock was divided in three depth intervals: 1227.01 - 1313.9 mbs; 1510.1 - 1511.72 mbs and, 1717.6 - 1720.37 mbs.

Two formations have been identified: Sleen and Aalburg Formation; based on lithological features and geochemical data (Fig. 22).

The Sleen Formation is represented in the lowermost interval (1717.6 - 1720.37 mbs) (Fig. 22). It is characterized by fine to coarse mudstone without ironstone horizons or nodules. At the top of the interval, a breccia bed has been described, but the origin is still uncertain (fault, transgressive surface…). Fossil content is not abundant (shell bioclasts), either bioturbation. This description concurs with the Sleen Formation in the Netherlands, performed by NAM & RGD 1980; van Adrichem Boogaert & Kouwe, 1993; and Dusar et al., 2001. Locally sandy claystone has been described in the upper part of the sequence, which has not been observed in the Molenbeersel cores recovered (NAM & RGD, 1980; van Adrichem Boogaert & Kouwe, 1994).

The Aalburg Formation is represented in the upper (1283.15 - 1313.9 mbs) and mid-interval (1510.1 - 1511.72 mbs) (Fig. 22). It is characterized by fine to coarse mudstone with ironstone horizons/nodules and calcite concretions. Sedimentary structures do not present high variability, lamination is dominant and some starved ripples have been described in the middle interval. Fossil content varies throughout the deposits being ammonites, shell bioclasts, gastropods, echinoderms, and belemnites the dominant ones. Some of the fossils are pyritized. Bioturbation is present in some areas, but not identified. The ironstones present a siderite composition and have been found throughout both intervals. This description concurs with the one performed for the Aalburg Formation in the Netherlands by NAM & RGD 1980; van Adrichem Boogaert & Kouwe, 1993; and Dusar et al., 2001.

Between the upper and mid interval, there is a gap of 196 m; between the mid and lower interval, there is a gap of 205 m. The boundary between the Sleen Formation (Rhaetian) and the Jurassic Aalburg Formation is suggested between the lower and mid intervals.

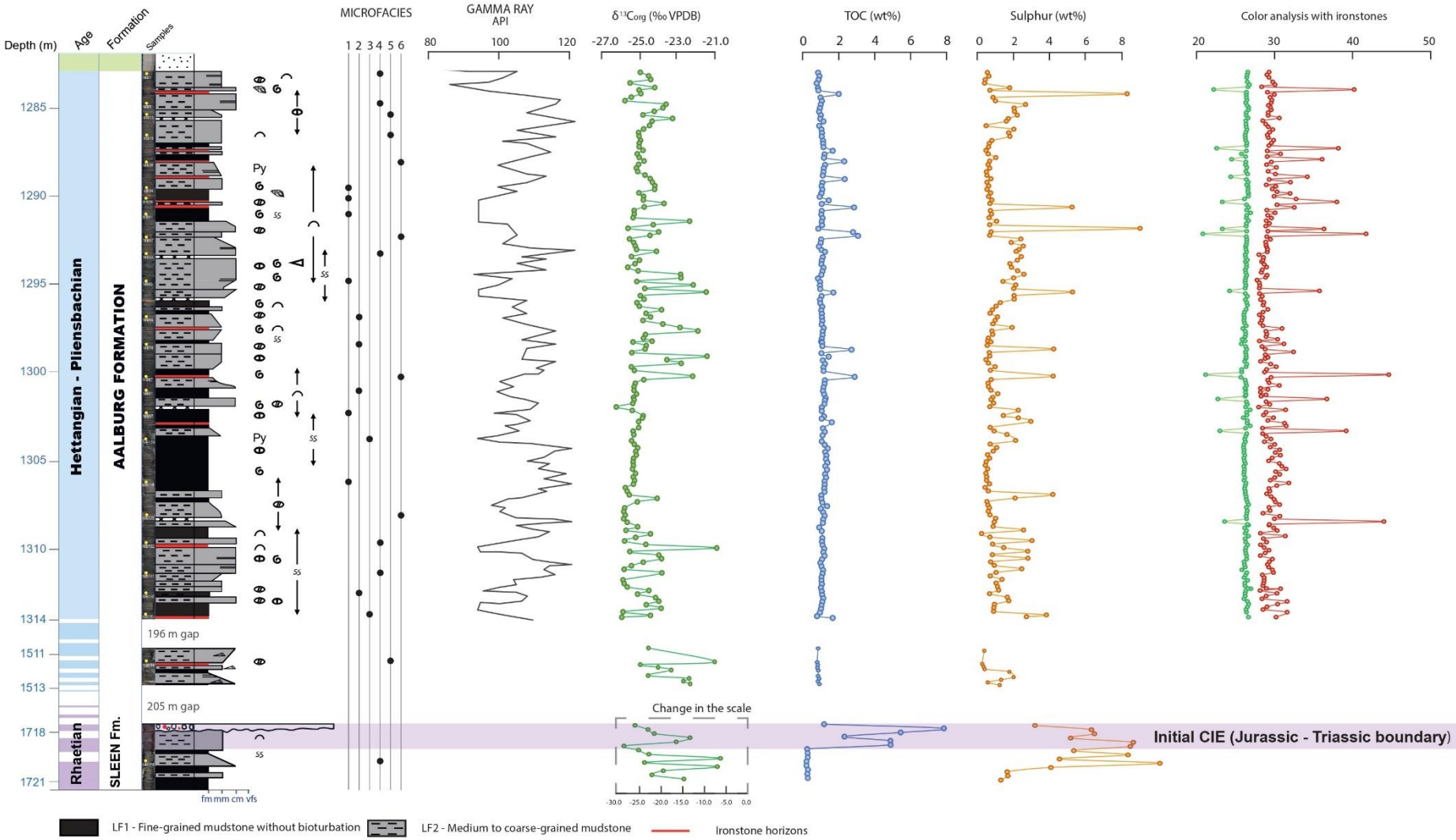

Fig. 22. Lithostratigraphic proposal**,** gamma ray (black), $\delta^{13}C_{org}$, (darker green), TOC (blue), sulfur (orange), and color analysis (550 nm WL- light green, 700 nm WL- red) of the Molenbeersel core. The gamma ray and color data are only available for the uppermost interval. The lithostratigraphic proposal is based on lithological features and TOC data. The Sleen Formation (Triassic) does not present ironstones. Furthermore, it presents a TOC anomaly, that is characteristic of the Triassic – Jurassic boundary. The Aalburg Formation is characterized by mudstones with siderite ironstones. The TOC shifts represent the ironstones.

The TOC data provides information that permits constraining the age represented in the Molenbeersel borehole. In the Upper Triassic – Lower Jurassic, two major carbon isotope excursions (CIE) have been described: the Triassic-Jurassic boundary (Hesselbo et al., 2000) and the Toarcian Oceanic Anoxic Event (T-OAE) (Jenkyns, 1988). Ruhl & Kürschner, (2010) studied the Triassic-Jurassic boundary in marine deposits from the Tethys Ocean located in Austria and described two distinct CIEs The actual CIE and an initial CIE below the actual boundary. They present a main negative CIE without a TOC anomaly and an initial CIE with a positive anomaly on the TOC (up to 8 wt%) (Fig. 23).

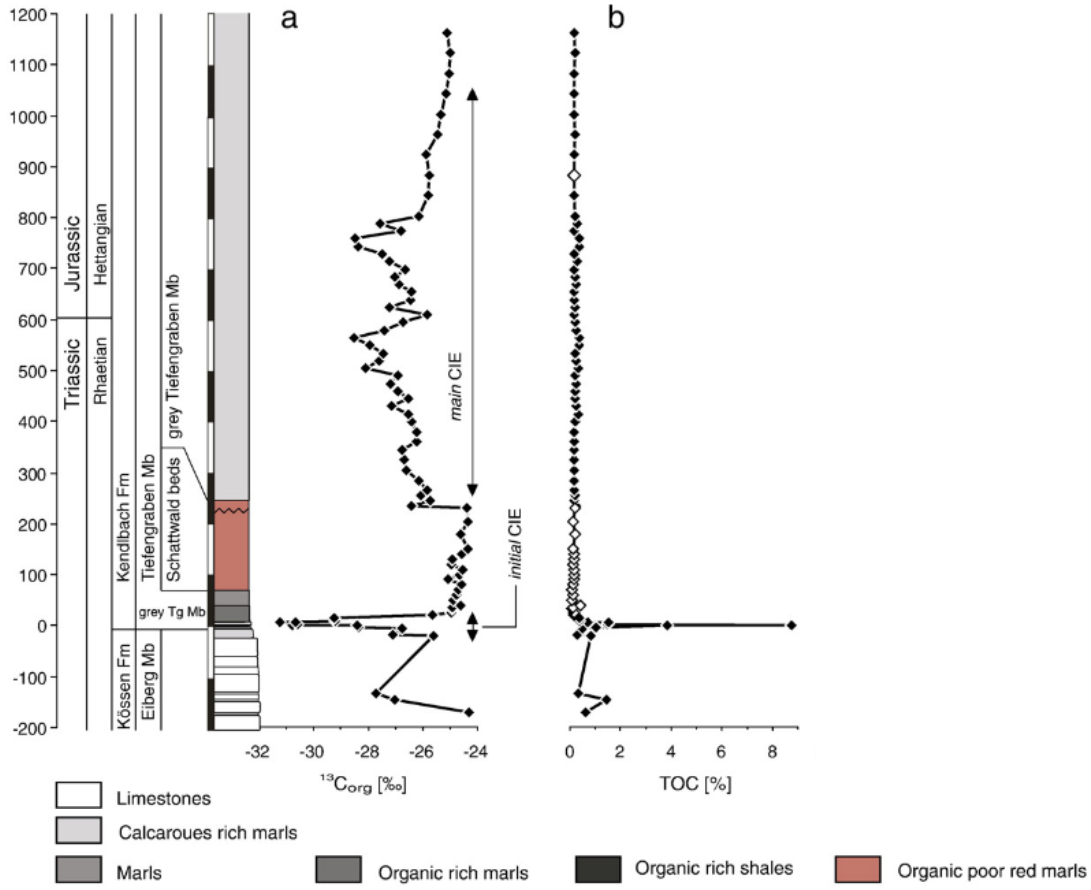

Figure 23. Geochemical proxy records of environmental change across the T–J boundary in the Kuhjoch section, Eiberg Basin (Austria). (a) The organic C-isotope signature [‰], (b) Total Organic Carbon content [%] (Modified from Ruhl & Kürschner, 2010).

The initial CIE anomaly in the TOC data from Ruhl, et al., (2010) displays a very similar trend as the TOC anomaly studied in the Sleen Formation of the Molenbeersel borehole, both reaching values higher than 8 wt%. It is suggested that the TOC excurison in the lowermost interval of the

Molenbeersel borehole comprises the initial CIE of the Triassic-Jurassic boundary. On the other hand, the $\delta^{13}C_{org}$ obtained from this core does not seem reliable, further measurements should be perform to verify the stratigraphic model propose above.

The second CIE in the Jurassic is the Toarcian Oceanic Anoxic Event (T-OAE), characterized by a negative $\delta^{13}C_{org}$ excursion and a positive TOC anomaly, due to an increase in the rate of burial of ^{13}C-depleted C_{org} caused by oceanic anoxia in the Laurasian Sea (Fig. 24) (Hesselbo et al., 2000; Kemp et al., 2005; French et al., 2014; McArthur et al., n.d.).

In the Molenbeersel borehole, the CIE and TOC anomaly from the T-OAE is not present, indicating that the deposits of the Molenbeersel borehole do not reach the age of the isotope anomaly.

In contrast to what the drilling company established (Edwin Maes, 1990), I propose that the deposits studied from the Molenbeersel borehole have a Upper Triassic – Lower Jurassic age (Fig. 24).

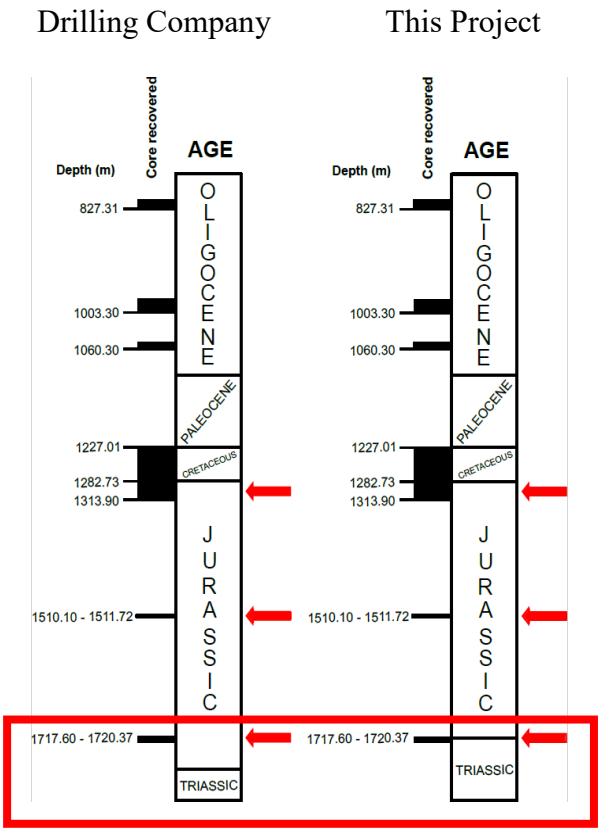

Fig. 24. New proposal on the age of the Molenbeersel deposits of this project. Marked with a red rectangle are the changes for the lowermost interval (1717.6 - 1720.37 mbs) from Lower Jurassic to Late Triassic (Modified from Edwin Maes, 1990).

5.2. Sedimentology of the Late Triassic – Early Jurassic in the Molenbeersel borehole and paleoenvironmental reconstruction

Mudstones from the Jurassic in the Laurasian Sea have been studied in detail by many researchers (Powell, 2010; Trabucho-Alexandre et al., 2022; Trabucho-Alexandre & Wong, 2024 and references therein), however, in the Molenbeersel borehole located in the Roer Valley Graben no research has focused in detail in the sedimentary and paleodepositional setting.

Sedimentary structures can offer important information about the sedimentary environment and the processes that lead to their formation (Lazar et al., 2015). In addition, bioturbation (biogenic sedimentary structures) and authigenic minerals can indicate paleoenvironmental conditions (bottom-water oxygenation levels, nutrients…).

In the Lower Jurassic of the Molenbeersel borehole, different sedimentary structures have been identified. Lamination in mudstones is a common sedimentary structure that offers information about the processes and environment that generated them (Potter et al., 2005; Lazar et al., 2015; Yawar & Schieber, 2017). In the Molenbeersel borehole the following sedimentary structures have been described:

Thin lamination with parallel geometry (continuous to discontinuous), by the accumulation of silt grains or interlamination of clay-silt grains during a continuous sedimentation period (Schieber & Southard, 2009)(Campbell, 1967). Lamination is formed by bedload transport (Schieber & Southard, 2009) indicating a low flow velocity (< 0.25 m/s) and a low sedimentation rate (Schieber & Southard, 2009; Schieber & Yawar, 2009; Schieber, 2011).

Small-scale cross lamination it has been described in some thin sections due to the contrast between components (Fig. 25A, 25B). O'Brien, (199)6 and Yawar & Schieber, (2017), suggest that small-scale cross-lamination is formed due to very low-velocity bottom currents, sometimes under anoxia, and with high sedimentation rates. The clay and silt are transported in aggregates.

Bed surfaces are found in all different grain sizes (fine, medium to coarse mudstone) (Fig. 16E, 16F). They present an irregular sharp base due to an erosive process that leads to the accumulation of coarse mud to very fine sand

grain size lag of quartz and bioclast debris (O'Brien, 1990, 1996). Above these structures, we observe a normal grading trend.

Normal Graded bedding is observed above erosional surfaces (Fig. 16E, 16F). During storms, coarse sediment (silt size, bioclasts…) is transported as bedload and deposited after the erosion of the sediment bed, fine-grained sediment remains suspended until the energy of the currents decreases and the finer components are deposited, leading to the normal grading trend (Figueiredo et al., 1982; Bastos et al., 2015),

The combination of the last two structures indicates local reworking of the sediment, where the coarse fraction is deposited first, and when the flow velocity decreases the smaller grain size fractions are deposited above (Schieber, 1999) (Fig. 16E, 16F). The absence of erosional surfaces described in some of the thin sections studied could be explain by periods of time of sedimentation without disturbances in the deposition. Alternatively, by the randomized location of the thin sections and the possibility of the presence of an erosional surfaces few cm above or below the thin section.

In many sections of the deposits we observe a massive appearance (lack of lamination). Three alternatives are discussed: 1) massive deposits due to dense gravity fluid deposits (Wilson & Schieber, 2014); 2) massive appearance due to very low contrast between the grains and elements of the mudstones that do not display lamination at first; 3) the grade of bioturbation is high enough (B. I. 6) that the primary lamination has been completely erased and the sediment has been homogenized. This last hypothesis implied a highly oxygenated bottom-water with low sedimentation rates (Droser & Bottjer, 1986). I suggest that there is probably a combination of all three hypothesis, however, considering the laminated appearance of the cores (Fig. 8), I am inclined towards the lack of lamination due to a lower contracts between the elements and grains of the mudstones.

Individual bioturbation (burrows) are observed in different parts of the core, usually around 1-2cm long (Fig. 13A, 13B). The presence of bioturbation indicates an oxygenated bottom-water condition.

The presence of some other components can provide great information on the depositional conditions and early diagenesis:

Organic matter is found in some thin sections, usually with the original geometry that has not been very deformed; which indicates early cementation of the deposits (Fig. 13C, Fig. 25C). The preservation of organic matter takes

place under dysoxic (low oxygen levels) or anoxic conditions. Many hypotheses have been proposed to explain this situation; Watanabe et al., 2007 propose that organic matter decomposition removes oxygen from the water column, when there is a high quantity of organic matter, the water column is stratified. In this setting, we can expect less or no bioturbation.

The presence of disarticulated fossils and bioclasts (gastropods, echinoids, ammonites, bivalves…) indicate that these components experienced transport before their deposition (not in life position) (Lazar et al., 2015). In the case of the Molenbeersel deposits, some of the fossils are unbroken and/or the edges of the bigger bioclasts are sharp, which suggests that the transport they suffered is not far from the source area (Fig. 25E).

In many of the samples studied, pyrite is present with different morphologies: framboidal, euhedral, big aggregates… It is the most common authigenic mineral found in the mudstone rock record (Berner, 1984). Pyrite forms in different conditions during early diagenesis due to bacterial reduction of dissolved sulfate into sulfide that reacts with the iron ions present (Berner, 1982). Pyrite can grow in oxic to anoxic-euxinic conditions (H_2O-bearing; O_2-depleted bottom waters) (Wilkin et al., 1996, 1997; Bond et al., 2004). In oxic conditions, the organic matter content is the major control in the formation (Berner, 1984). In euxinic conditions, the dominant control is the Fe^{2+}; in this setting, higher content of pyrite is found in the deposits (Berner, 1984). In the Molenbeersel cores, pyrite is found with different morphologies, which brings information about their growth conditions:

· Euhedral: authigenic pyrite can be formed in two ways: 1) direct, little organic matter supplies (Berner, 1982); 2) indirect, fromboidal pyrite undergoes regrowth during diagenesis (Cavalazzi et al., 2012).

· Framboid: very typical texture of sedimentary pyrite in marine conditions (Rickard, 2012). They are densely packed spherical aggregates of microcrystals of pyrite (Love & Amstutz, 1966). The size of the framboids can be used to interpret the oxygenation level of the bottom waters (Wilkin et al., 1997; Wignall & Newton, 1998). If the framboids present a small diameter (< 5 μm), it is an indicator of euxinic conditions (Wignall & Newton, 1998; Wang et al., 2012; Chang et al., 2022). If the framboids present a diameter of < 10 μm, it has been interpreted as an indicator of anoxic-dysoxic environments (Wang et al., 2012; Chang et al., 2022).

Pyrite can also be found replacing the internal structure of bioclasts (usually the soft structure), due to the oxidation of organic matter within the fossil (Fisher, 1986; Canfield, 1991) (Fig. 25F).

Gathering the information above with the pyrite geometries present in the Molenbeersel cores, we can expect periods of anoxic or euxinic conditions. In some thin sections, pyrite grows following the primary lamination, which could indicate the presence of accumulated organic matter that triggered the growth of the mineral (Fig. 17D**)**. On the other hand, it has been described the presence of higher energy currents that reworked material, authigenic pyrite is expected to be reworked as well in some of the sections studied. Further research is recommended to study in detail the changes in the abundance and diameter of the pyrites for a more detailed interpretation of the paleoenvironmental conditions.

Another important diagenetic component found in the Molenbeersel borehole are carbonate concretions and nodules. Some of them grew around a nucleus (bioclast) and present a clear rounded shape (Fig. 17C, 25C). This is common due to the release of ammonia from the fossil due to the decaying organic matter that alters the pH and allows the calcite cement to precipitate (Prothero & Schwab, 1996). In anoxic conditions, bacterial sulfate reduction takes place, pyrite grows and increases alkalinity levels and can induce calcite precipitation (Berner et al., 1970).

Siderite concretions are common in the Aalburg Formation, and their formation will be discussed in section *5.2.1.*

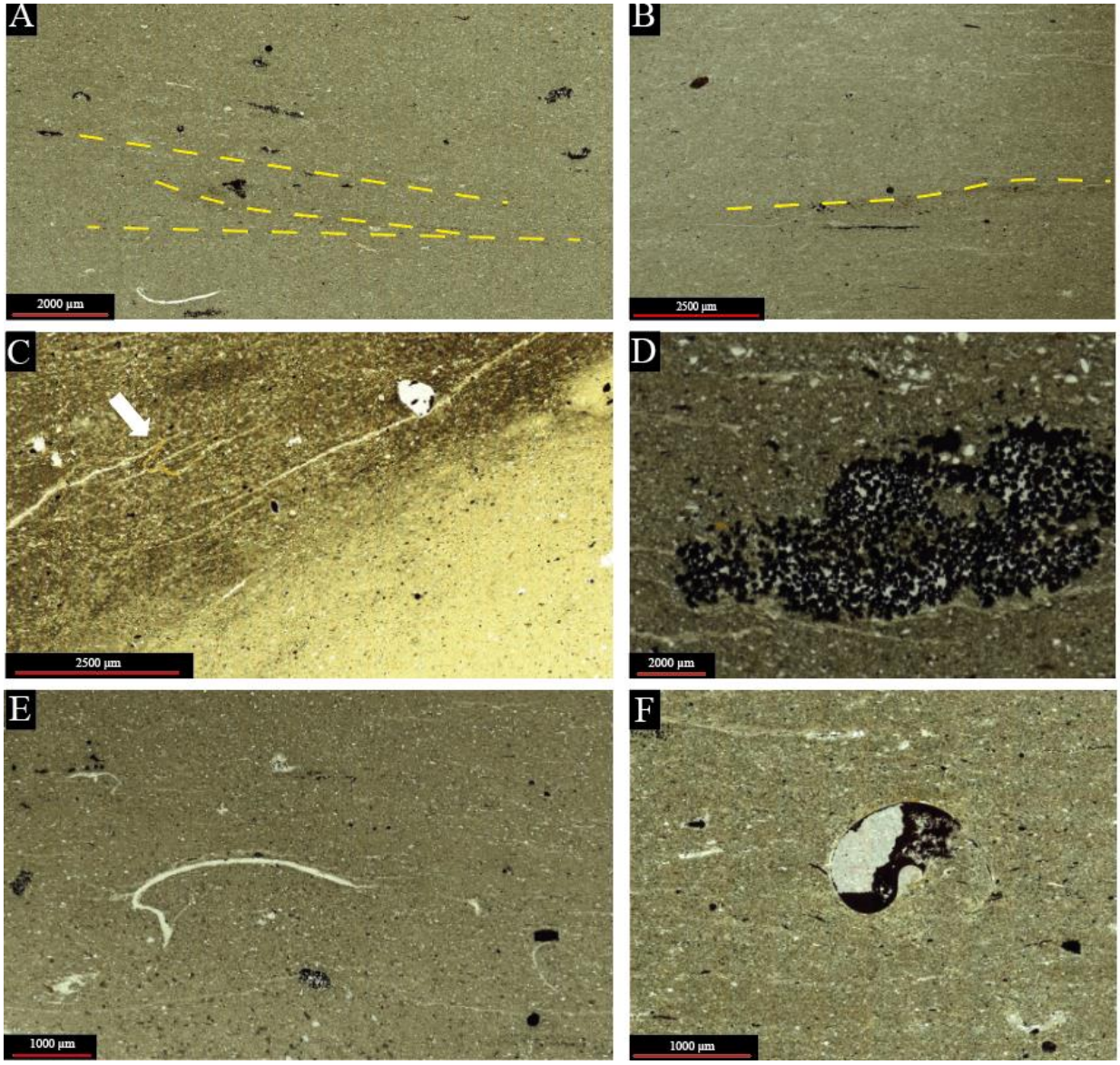

Fig. 26. Different sedimentary structures and components of the Lower Jurassic of the Molenbeersel borehole. **A)** Small-scale cross lamination, the cross-bedding geometry is indicated with dashed yellow lines (MB36; 1290.15 mbs**). B)** Small-scale ripple, it is possible to distinguish it due to the contrast between grains, indicated with a yellow dashed line (MB146; 1312.40 mbs). **C)** Calcite concretion in the lower-right corner, presenting a smaller grain size and a lighter color. Unflatten organic matter with an orange color, indicated by a white arrow; indicates early cementation (MB13; 1285.55 mbs**). D)** Pyrite aggregate confirmed by smaller framboidal pyrites (MB69; 1296.75 mbs). **E)** Sharp edges of a bioclast; indicative of little transport from the source area (MB69; 1296.75mbs). **F)** Pyrite growth inside an ammonite bioclast, the original internal structure is not preserved (MB9; 1284.75 mbs).

5.2.1. Ironstone horizons and concretions

Ironstones in the Molenbeersel borehole are found in the Aalburg Formation (1283.15 ~ 1511.72 mbs) in two forms: as horizons from 3 cm to 10 cm thick approximately, and as small rounded or elongated nodules. They present a characteristic red color, and in some cases, septarian calcite veins, typically in the horizons. The ironstones are composed mainly of siderite ($FeCO_3$), quartz, calcite, and kaolinite (Fig. 14B).

When studying the TOC data of the ironstones, they present a higher value (2.81 wt%) compared to the mudstones. When correlating these higher peaks to the color data (only in the uppermost interval), it is confirmed that the higher TOC peaks correspond to the red 700 nm WL peaks (Fig. 26, red highlight). In the figure, it can be seen that some 700 nm WL peaks do not correspond to TOC peaks (orange highlight); this can be explained by the randomized sample selection. Some of the sulfur peaks match as well with the TOC – 700 nm red peaks, but not all of them; between the depths of 1290 – 1285 mbs, the ironstone peaks do not show a sulfur peak.

Ironstones have been used for depositional environment interpretations since siderite forms during early diagenesis and provides great information about the environmental conditions (OERTEL & CURTIS, 1972; Mozley, 1989; Browne & Kingston, 2003; Akinlotan, 2019). Siderite concretions grow under anoxic and reduced conditions; Fe^{2+} reacts with carbonate ions (CO_2) to form ironstones. Under oxic conditions, the iron ion would be oxidized (Huber, 1958; Loope et al., 2012; Bachan & Kump, 2015; Akinlotan, 2019). Akinlotan, (2017) claims that the composition of the host rock might have an important control on the composition of the siderite ironstone. In the Lower Jurassic of the Molenbeersel borehole, the XRD diffractograms of the ironstones show a very similar mineral association as the mudstones (quartz and kaolinite), suggesting that during diagenesis, siderite replaced part of the deposited detrital facies by siderite under anoxic conditions.

Many authors (Van Lith et al., 2003; Sel et al., 2012; Roberts et al., 2013) proposed the participation of microbes (bacterial iron reducers), which would dissolve iron and induce alkaline condition.

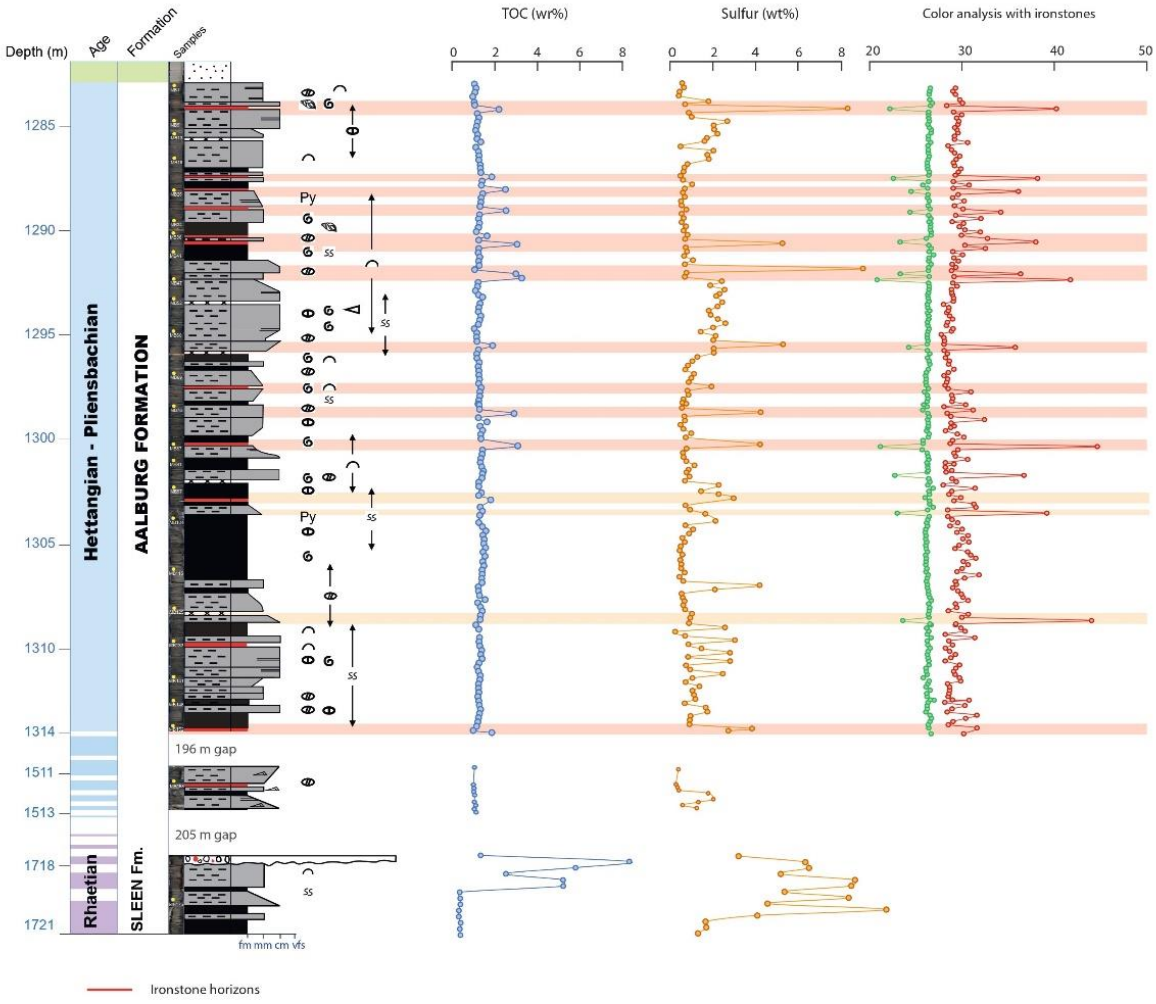

Fig. 26. TOC, sulfur, and color data (550 nm WL, 700 nm WL) of the uppermost interval (1283.15 - 1313.9 mbs) of the Lower Jurassic at the Molenbeersel borehole. The red highlight indicates the matching peaks of the WL700 (red) and TOC data. The orange highlight indicates the non-matching peaks between the same two variables; this is interpreted to be explained by the sampling selection.

5.2.2. Paleoenvironmental reconstruction

The Upper Triassic – Lower Jurassic Molenbeersel rocks were deposited in the Laurasian Sea, an epeiric sea that occupied the western part of modern Europe (Doornenbal & Stevenson, 2010).Most of the deposits formed during this time are marine mudstones, fine-grained deposits formed by different % of quartz, clay minerals, bioclast debris, and organic matter.

It has been suggested that mudstones can be deposited in rather dynamic depositional settings, contrary to what was previously thought (Schieber, 1999; Sageman et al., 2003; Macquaker et al., 2007).

The Molenbersel mudstones were deposited in a hemipelagic shallow marine setting where higher energy currents reworked the sediments. Trabucho-Alexandre et al., 2022; studied similar but coarser-grained mudstone deposits (lower Toarcian mudstones) from the Yorkshire coast, describing comparable sedimentary structures and establishing storm-driven bottom currents responsible for sediment erosion, transport, and deposition during that period of time. The sedimentary structures, textures, and fabrics show changes in the processes affecting the deposits. Trabucho-Alexandre et al., (2022) and Trabucho-Alexandre & Wong, (2024) suggest that the water depth in the Laurasian Sea has been in general overestimated, and sedimentary structures during the Toarcian indicate that the seafloor of the southern North Sea was above storm wave base (Pye & Krinsley, 1986; Mitchell et al., 2011; Dera & Donnadieu, 2012; Trabucho-Alexandre et al., 2012, 2022; Trabucho-Alexandre, 2015). This approach could be extrapolated to the Roer Valley Graben, due to the similar tectonic evolution and depositional setting. On the other hand, the sedimentary features of the Toarcian mudstones studied by Trabucho-Alexandre et al., (2012) display a more heterogeneous texture and higher variety of structures, which could suggest that the Roer Valley Graben, was indeed a deeper basin.

The bottom-water oxygenation was rather dynamic; the deposits studied exhibit evidence of both, oxygenated bottom-waters and dysoxic – anoxic – euxinic bottom-waters. The presence of bioturbation indicates the occurrence of organisms living and altering the sediments of the sea floor. On the other hand, the existence of authigenic minerals such as pyrite and siderite indicates that periods of time of relatively lower oxygen levels, anoxia, or euxina took place during the deposition of the Upper Triassic – Lower Jurassic rocks in the Molenbeersel borehole. These bottom-water changes could have been triggered by different causes such as sea level fluctuations, water circulation dynamics, or primary productivity (Pye & Krinsley, 1986; Elsayed, 2021). This environmental setting hypothesis is supported by the higher TOC level in some parts of the deposits, which they could only be preserved under reducing conditions.

The TOC peaks (associated to the ironstones) (Fig. 27) are interpreted as an indicative of periods of time of lower to non-sedimentation. This would allow the accumulation of organic carbon in the sea floor, followed by higher sedimentation intervals, which buried those beds.

Lott et al., (2010) state that during the deposition of the Aalburg Formation, an important marine transgression took place. Thus, the Roer Valley Graben experienced a relative deepening compared to the Rhaetian, Sleen Formation.

5.3. Correlation to other Lower Jurassic deposits of NW Europe

5.3.1. Thickness changes inside the RVG

In the Roer Valley Graben, other boreholes have shown the presence of the Altena Group (data from the Dutch Oil and Gas Portal - NLOG). To study the heterogeneity or homogeneity of the thicknesses, I compared the thicknesses and presence of the lowermost units of the Altena Group (Sleen, Aalburg, and Posidonia Shale Formations) in other parts of the basin. In the eastern part, the presence of these formations has not been described; however, stratigraphic lower units are present, indicating the absence of the Altena Group. In the western part of the basin, geographically closer to the Molenbeesel borehole, some of the Formations of the Altena Group are present. Table 5 summarizes the thickness information of the formations that are present in a few boreholes; a high heterogeneity is observed. The Posidonia Shale Formation is not found in all the boreholes; the Aalburg Formation is present in most of the boreholes of the western part of the Roer Valley Graben but with a thickness ranging between 5 to 700 m; the Sleen Formation is almost present in all the boreholes of the area with a lower thickness range. The presence or absence, and thickness changes of the Altena Group is interpreted as differential subsidence rates inside the basin, the erosion of the deposits after the inversion events, and probably the presence of faults that could impact the thicknesses.

			Thickness (meters)		
Well name	**x-coord (WGS84)**	**y-coord (WGS84)**	**Posidonia Shale Fm.**	**Aalburg Fm.**	**Sleen Fm.**
VELDHOVEN-01	51.4383112	5.35906948	46.00	18.00	
NEDERWEERT-01	51.31080179	5.76949409		5.00	23.00
ASTEN-01	51.39579486	5.78968568		412.00	17.00
KELDONK-01	51.58144704	5.59816156		105.00	25.00
BROEKZIJDE-01	51.52090649	5.19516788	34.12	233.35	46.00

HILVARENBEEK-01	51.5046006	5.11675361	28.00	330.00	20.50
SINT-MICHIELSGESTEL-01	51.64763124	5.37148166	31.26	703.10	31.00
HEESWIJK-01	51.66344722	5.4458024		264.00	30.00

Table 5. Thickness comparison in other boreholes of the west Roer Valley Graben, Netherlands. (Data from the Dutch Oil and Gas Portal)

3.5.2. Correlation with the Netherlands

Two important Cimmerian basins from the Netherlands have been compared to the Roer Valley Graben in order to study the differences and similarities in the Triassic-Jurassic deposits.

The West Netherlands Basin is a Cimmerian Basin located west of the Roer valley Graben (Fig. 2) and it underwent a very similar tectonic evolution (Herngreen et al., 2003; Lott et al., 2010). Table 6 presents a summary of the thickness variability in some boreholes from different parts of the basin. As it can be seen, the Altena Group formations presents the same heterogeneity that has been described in Table 5.

			Thickness (meters)		
Well	**x-coord (WGS84)**	**y-coord (WGS84)**	**Posidonia Shale Fm.**	**Aalburg Fm.**	**Sleen Fm.**
SPRANG CAPELLE-01	51.71027335	4.99951918	14	73	44.5
DONGEN-01	51.62614752	4.91212517		59	
MEERKERK-01	51.9256656	4.97713133	42.05	398.43	48
AARLANDERVEEN-01	52.16162393	4.74014724		284	31
WILLESKOP-01	52.01737382	4.8866714	38.63	440.69	181
HAARLEMMERMEER-01	52.24125493	4.67865303	34	61.8	
OEGSTGEEST-01	52.19677274	4.47329694	28	30	

Table 6. Thickness comparison in some boreholes of the West Netherlands Basin, Netherlands (Data from the Dutch Oil and Gas Portal).

The Dutch Central Graben is another Cimmerian basin located in the North Sea; it is a major N-S oriented rift system developed during the Early Cimmerian tectonic phase (Fig. 2) (Herngreen et al., 2003; Lott et al., 2010). Table 7 summarizes the thickness ranges in some boreholes inside the basin; we observe the same heterogeneity of thickness in the Aalburg Formation. In many boreholes, the Altena Group is not present.

			Thickness (meters)		
Well	**x-coord (WGS84)**	**y-coord (WGS84)**	**Posidonia Shale Fm.**	**Aalburg Fm.**	**Sleen Fm.**
F11-01	54.36706184	4.59279517	37.06	276.75	
F14-05	54.26236056	4.54332226		76.5	
L05-04	53.81779134	4.40233542	21.32	25.68	
L05-03	53.82212455	4.38047363	22.86	29.27	
F17-04	54.0603831	4.43563423		69	

Table 7. Thickness comparison in some boreholes of Dutch Central Graben, Netherlands (Data from the Dutch Oil and Gas Portal).

This data shows that the West Netherlands Basin, adjacent to the Roer Valley Graben, presents similarities in the thickness and presence of the formations, indicating they underwent similar depositional and tectonic evolution. Wong, (2007) claimed that the impact of the uplift in the West Netherlands Basin and the Roer Valley Graben was not as intense compared to other Cimmerian basins and deposition was rather continuous until the Oxfordian.

In the Dutch Central Graben, the Aalburg Formation presents great changes in thickness. The deposits have been studied in deeper detailed and described as dark grey to clay claystones with fossils that may be pyritized (Wong, 2007). Trabucho-Alexandre et al., (2012) studied two cores from the area and described the deposits as bioturbated coarser-grained facies deposited during a periods of higher influx of terrigenous sediments. The Sleen Formation is more absent compared to the southern basins.

Combining the information, it is suggested that the West Netherlands Basin and the Roer Valley Graben underwent very similar sedimentary and tectonic evolution, whereas the Dutch Central Graben was shallower and underwent higher uplift and erosion rates during the Jurassic that lead to a more discontinuous record.

5.3.2. Correlation with United Kingdom

The Lower Jurassic in the UK is represented by the Lias Group (Hettangian to Toarcian) (SMITH, 1797; Powell, 2010 and references therein); characterized by marine mudstones, deposited in an epeiric shallow sea (Laurasian Sea) (Lott et al., 2010). This section focuses on the comparison of the Roer valley Graben Lower Jurassic deposits with the Cleveland Basin.

The Cleveland Basin is an extensional basin formed during the Early Cimmerian tectonic phase, located in North Yorkshire, North-East England (Bradshaw et al., 1992; Rawson & Wright, 1995; Simms et al., 2004; Powell, 2010). It was connected to the Sole Pit Basin and the West Netherlands Basin (Powell, 2010 and references therein). This basin experienced subsidence during the Early Jurassic, permitting the deposition of the Lias Group (Rawson & Wright, 1995). During the Middle Jurassic, compressional events lead to erosion of the upper part of the Lias deposits (Hemingway, 1974).

The Lias Group has been studied in depth with offshore cores and outcrops from the Yorkshire coast (Trabucho-Alexandre et al., 2022 and references therein). Since the Lias Group and the Altena Group were deposited in similar environments, a correlation between the lithostratigraphic units is possible, summarized in Figure 27**.** The Sleen Formation correlates to the Westbury Formation of the Penarth Group (Benfield & Warrington, 1988; Ivimey–Cook & Powell, 1991; Powell, 2010); the Aalburg Formation correlates to the Redcar Mudstone Formation, Staithes Sandstone Formation, and the Cleveland Ironstone Formation (Powell, 2010). The Posidonia Shale Formation corresponds to the Whitby Mudstone Formation (Powell, 2010). In the last mentioned formation, the T-OAE is found at the bottom of the Mulgrave Shale Mbr (Jenkyns, 1988).

<table>
<tr><th colspan="2">CHRONOSTRATIGRAPHY</th><th colspan="3">CLEVELAND BASIN (UK)</th><th>BELGIUM - NETHERLANDS</th></tr>
<tr><td>Series</td><td>Stage</td><td colspan="3">Powell (1984) and Knox (1984)</td><td>Adrichem Boogaert & Kouwe, 1994–1997; Herngreen et al., 2003</td></tr>
<tr><td>Middle Jurassic</td><td>Aalenian</td><td rowspan="12">Lias Gr.</td><td colspan="2">Erosion surface</td><td rowspan="3">Werkendam Formation</td></tr>
<tr><td rowspan="5">Lower Jurassic</td><td rowspan="4">Toarcian</td><td rowspan="2">Blea Wyke Sandstone Fm.</td><td>Yellow Sandstone Mb.</td></tr>
<tr><td>Grey Sandstone Mb.</td></tr>
<tr><td rowspan="5">Whitby Mudstone Fm.</td><td>Fox Cliff Siltstone Mb.</td><td rowspan="4">Posidonia Shale Formation</td></tr>
<tr><td>Peak Mudstone Mb.</td></tr>
<tr><td>Alum Shale Member</td></tr>
<tr><td>Mulgrave Shale Mb.</td></tr>
<tr><td rowspan="6">Pliensbachian</td><td>Grey Shale Mb.</td><td rowspan="6">Aalburg Formation</td></tr>
<tr><td colspan="2">Cleveland Ironstone Formation.</td></tr>
<tr><td colspan="2">Staithes Sandstone Fm.</td></tr>
<tr><td rowspan="4">Redcar Mudstone Fm.</td><td>Ironstone Shales</td></tr>
<tr><td>Pyritous Shales</td></tr>
<tr><td>Siliceous Shales</td></tr>
<tr><td>Calcareous Shales</td></tr>
<tr><td>Sinemurian</td><td colspan="3"></td></tr>
<tr><td>Hettangian</td><td colspan="3"></td></tr>
<tr><td>Upper Triassc</td><td>Rhaetian</td><td colspan="2">Penarth Group</td><td>Sleen Formation</td></tr>
</table>

Fig. 27. Stratigraphical framework for the Lower Jurassic Lias Group in the Cleveland Basin (after Powell 1984; Knox 1984; Rawson & Wright 2000) and the Belgium – Netherlands nomelanclature used in the Roer Valley Graben (After Adrichem Boogaert & Kouwe, 1994–1997; Herngreen et al., 2003).

When comparing the average thicknesses between the formations, the Redcar Mudstone, Staithes Sandstone, and the Cleveland Ironstone Formations (corresponding to the Aalburg Formation), present an average thickness of 310 m in the Cleveland Basin (O'B Knox, 1984; Powell, 1984; Rawson & Wright, 2000). In the Molenbeersel borehole, the Aalburg Formation reaches up to ~ 433 m thick, assuming that the lowermost interval is the Sleen Formation (Rhaetian). That indicates a thickness difference of 123 m between the Cleveland Basin and the Roer Valley Graben.

Trabucho-Alexandre et al., (2022) studied the Toarcian deposits and T-OAE in the Cleveland Basin. When comparing our results to Figure 28, we observe that in the Moleneersel borehole, the $\delta^{13}C_{org}$ and TOC Toarcian excursion is not present, meaning that the deposits do not reach the age of the T-OAE . However, in the Yorkshire coast outcrop lithology log in Figure 28, before the carbon isotope excursion, the mudstone deposits present ironstone nodules

(between 48 – 58 m in Fig. 28), similar to what has been described at the Molenbeersel borehole.

Taking into account the thickness difference and the similarities in the deposits, the Lower Jurassic Molenbeersel deposits could reach an age up to Lower Toarcian, below the T-OAE, meaning that the Pliensbachian – Toarcian boundary and the lower part of the Posidonia Shale Formation might be present in the Molenbeersel borehole.

On the other hand, when comparing the TOC and $\delta^{13}C_{org}$ data, a negative CIE has been described at the Pliensbachian – Toarcian boundary (Hesselbo et al. 2000; Trabucho-Alexandre et al., 2022), which is not present in the upper part of the Molenbeersel borehole. In some deposits, the CIE displays a positive anomaly on the TOC data (38 m at the Yorkshire coast outcrop of Fig. 28), but that is not present in every Pliensbachian – Toarcian boundary studied (185 m in the Dove's Nest core from Fig. 28). This leaves room for further investigations in the topic.

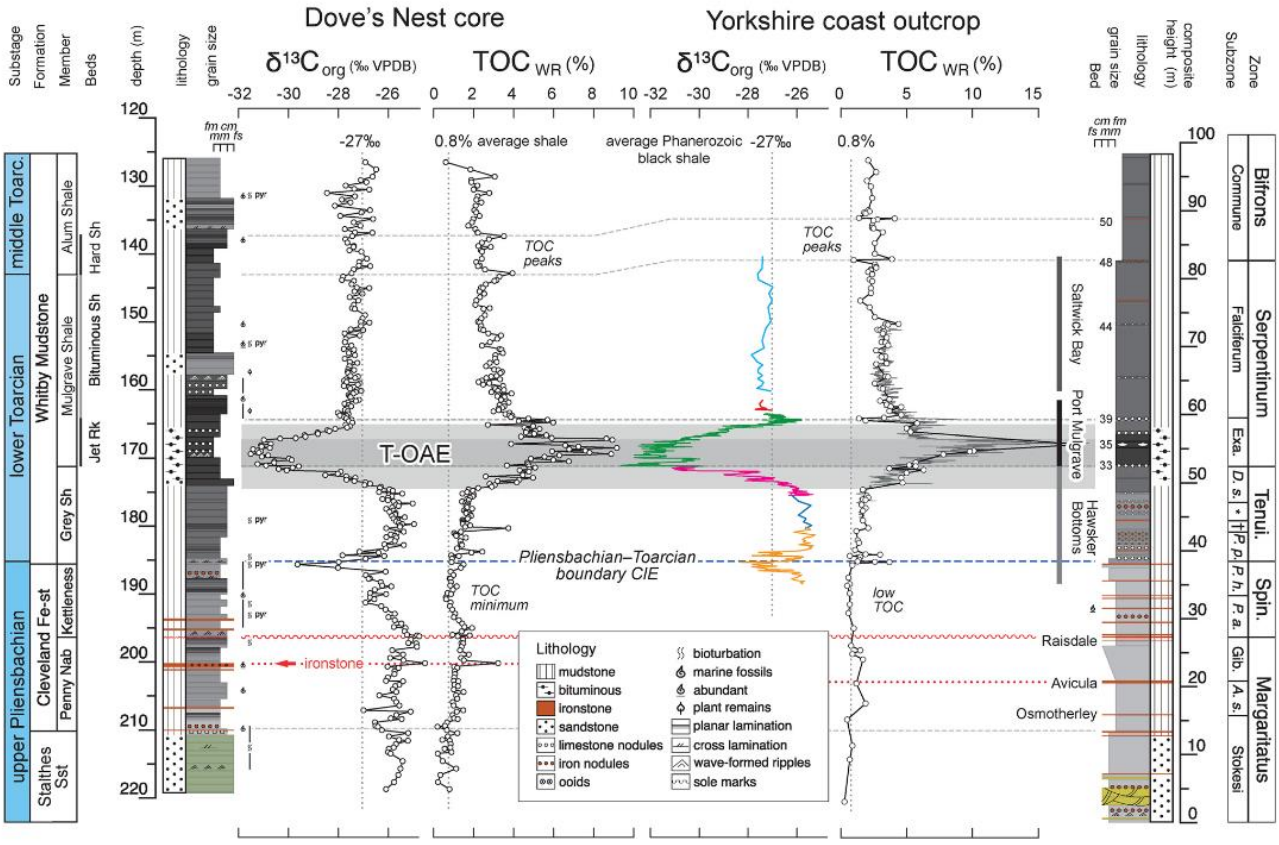

Fig. 28. Stratigraphic log of the studied section of Dove's Nest core (left) and of the correlative composite outcrop section along the North Yorkshire coast between Hawsker Bottoms and Port Mulgrave (right; Fig. 1). Organic carbon isotopes ($\delta 13C_{org}$) and whole-rock total organic carbon (TOC_{WR}) profiles are shown with their correlation. Grain size scale: fm, fine mudstone; mm, medium mudstone; cm, coarse mudstone; fs, very fine sandstone. Yorkshire coast 'bed' numbers from Port Mulgrave after Howarth (1962, 1992); named marker beds after Howarth (1955).Dove's Nest data from this study. Yorkshire coast δ13Corg data from Hawsker Bottoms: orange, Littler et al. (2010); blue, Cohen et al. (2004); pink, Kemp et al. (2005). Port Mulgrave: green, Kemp et al. (2005); red, Cohen et al. (2004). Saltwick Bay: cyan, Cohen et al. (2004). TOC data for the Yorkshire coast are composite section values after McArthur (2019; thick line with unfilled circles) and Kemp et al. (2011; thin grey high-resolution curve). Abbreviations of biostratigraphic zonation: Tenui. = Tenuicostatum; Spin. = Spinatum; Exa. = Exaratum; D. s. = Semicelatum; * = Tenuicostatum; † = Clevelandicum; P. p. = Paltum; P. h. = Hawskerense; P. a. = Apyrenum; Gib. = Gibbosus; A. s. = Subnodosus (Trabucho-Alexandre et al., 2022).

6. Conclusion

In the deposits studied from the Molenbeersel borehole, two formations from the Altena Group have been identified. The Sleen Formation deposited during the Rhaetian (Upper Triassic) in the lowermost interval (1717.6 - 1720.37 mbs), characterized by mudstones without ironstones. The Aalburg Formation, deposited between the Hettangian ~ Pliensbachian (Lower Jurassic), has been identified in the mid and uppermost intervals. The Aalburg Formation is characterized by laminated mudstones with ironstone horizons and calcite concretions throughout the deposits.

The recognition of the formations has been established by the study of lithological features, $\delta^{13}C_{org}$, and TOC data. TOC offers information in both, lithostratigraphy and depositional environment setting. The TOC positive excursion (~ 8 wt%) located at the lowermost interval (top of Sleen Formation), represents the initial CIE and TOC anomaly that characterizes the Triassic – Jurassic boundary (Ruhl & Kürschner, 2010).

The deposition of the Molenbeersel borehole deposits during the Upper Triassic – Lower Jurassic took place in the Laurasian Sea, in a shallow marine epeiric setting. The presence of sedimentary structures such as lamination, small-scale cross-bedding, bed surfaces, normal grading, and bioturbation indicates the deposition in hemipelagic setting with the interruption of storm-driven currents(higher energy currents) which eroded and re-worked the

sediments. The positive peaks of TOC in the Aalburg Formation indicates periods of time of little to no-sedimentation, when the organic carbon had sufficient time to accumulate in those layers.
The environment was rather dynamic since there is evidence of oxygenated periods (bioturbation) and dysoxic – anoxic – euxinic periods (authigenic minerals; pyrite and siderite). The changes in environmental conditions could be triggered by sea level fluctuations, changes in water circulation, or primary productivity oscillations (Morris, 1980**;** Pye and Krinsley 1986).

This setting is not limited to the Roer Valley Graben, other Cimmerian basins that underwent comparable tectonic and environmental evolution present similar characteristics in lithology and thickness of the deposits, such as the West Netherland Basin.

However, other basins located in the Laurasian Sea area present differences, such as coarser-grained deposits and sedimentary structures that indicate shallower marine conditions compared to the Roer valley Graben deposits of the Molenbeersel borehole, like the Dutch Central Graben. These distinctions can be explained by differential subsidence during deposition and different uplift and erosion rates (Ziegler, 1990; Herngreen et al., 2003).

Lastly, the comparison between the Roer Valley Graben and the Cleveland basin deposits offers the possibility to extend the lithostratigraphic model and age of the Molenbeersel borehole deposits, initially proposed in this project. The Aalburg Formation correlates to the Redcar Mudstone Formation, Staithes Sandstone Formation, and the Cleveland Ironstone Formation from the Cleveland basin. Comparing the thicknesses, it is noticed that the Molenbeersel borehole is 123 m thicker than the average thickness of the three formations mentioned above. In the Yorkshire coast, the Whitby Mudstone Formation, which correlates to the Posidonia Shale Formaiton in the Netherlands-Belgium subsurface, presents ironstones just below the T-OAE. This information offers the possibility of extending the upper age boundary of the Molenbeersel borehole deposits up to the Lower Toarcian.

6. References

Akinlotan, O., 2019. Sideritic ironstones as indicators of depositional environments in the Weald Basin (Early Cretaceous) SE England. Geological Magazine **156**(3): 533–546. doi: 10.1017/S0016756817001017

Bachan, A. & Kump, L.R., 2015. The rise of oxygen and siderite oxidation during the Lomagundi Event. Proceedings of the National Academy of Sciences **112**(21): 6562–6567. doi: 10.1073/pnas.1422319112

Bastos, A.C., Quaresma, V.S., Marangoni, M.B., D'Agostini, D.P., Bourguignon, S.N., Cetto, P.H., Silva, A.E., Amado Filho, G.M., Moura, R.L. & Collins, M., 2015. Shelf morphology as an indicator of sedimentary regimes: A synthesis from a mixed siliciclastic–carbonate shelf on the eastern Brazilian margin. Journal of South American Earth Sciences **63**: 125–136. doi: 10.1016/j.jsames.2015.07.003

Benfield, A.C. & Warrington, G., 1988. New records of the Westbury Formation (Penarth Group, Rhaetian) in North Yorkshire, England. Yorkshire Geological Society **47**: 29–32.

Berner, R.A., 1982. Burial of organic carbon and pyrite sulfur in the modern ocean: its geochemical and environmental significance. Am. J. Sci.; (United States) **282**. doi: 10.2475/ajs.282.4.451

Berner, R.A., 1984. Sedimentary pyrite formation: An update. Geochimica et Cosmochimica Acta **48**(4): 605–615. doi: 10.1016/0016-7037(84)90089-9

Berner, R.A., Scott, M.R. & Thomlinson, C., 1970. Carbonate Alkalinity in the Pore Waters of Anoxic Marine Sediments1. Limnology and Oceanography **15**(4): 544–549. doi: 10.4319/lo.1970.15.4.0544

Bond, D., Wignall, P.B. & Racki, G., 2004. Extent and duration of marine anoxia during the Frasnian–Famennian (Late Devonian) mass extinction in Poland, Germany, Austria and France. Geological Magazine **141**(2): 173–193. doi: 10.1017/S0016756804008866

Bradshaw, M.J., Cope, J.C.W., Cripps, D.W., Donovan, D.T., Howarth, M.K., Rawson, P.F., West, I.M. & Wimbledon, W.A., 1992. Jurassic : in Atlas of Palaeogeography and Lithofacies. 107–129.

Browne, G.H. & Kingston, D.M., 2003. Early Diagenetic Spherulitic Siderites from Pennsylvanian Palaeosols in the Boss Point Formation, Maritime Canada. *In*: Sandstone Diagenesis. John Wiley & Sons, Ltd: pp. 223–230. doi: 10.1002/9781444304459.ch9

Callomon, J.H., 2003. The Middle Jurassic of western and northern Europe: its subdivisions, geochronology and correlations. GEUS Bulletin **1**: 61–73. doi: 10.34194/geusb.v1.4648

Canfield, D.E., 1991. Pyrite formation and fossil preservation. Taphonomy: releasing the data locked in the fossil record. Topics in Geobiology **9**: 337–387.

Cavalazzi, B., Barbieri, R., Cady, S.L., George, A.D., Gennaro, S., Westall, F., Lui, A., Canteri, R., Rossi, A.P., Ori, G.G. & Taj-Eddine, K., 2012. Iron-framboids in the hydrocarbon-related Middle Devonian Hollard Mound of the Anti-Atlas mountain range in Morocco: Evidence of potential microbial biosignatures. Sedimentary Geology **263–264**: 183–193. doi: 10.1016/j.sedgeo.2011.09.007

Chang, J., Li, Y. & Lu, H., 2022. The Morphological Characteristics of Authigenic Pyrite Formed in Marine Sediments. Journal of Marine Science and Engineering **10**(10): 1533. doi: 10.3390/jmse10101533

Deckers, J., Rombaut, B., Van Noten, K. & Vanneste, K., 2021. Influence of inherited structural domains and their particular strain distributions on the Roer Valley graben evolution from inversion to extension. Solid Earth **12**(2): 345–361. doi: 10.5194/se-12-345-2021

Demyttenaere, R., 1989. The post-Paleozoic geological history of north-eastern Belgium. Schone Kunsten België **51**: 51–81.

Dera, G. & Donnadieu, Y., 2012. Modeling evidences for global warming, Arctic seawater freshening, and sluggish oceanic circulation during the Early Toarcian anoxic event. Paleoceanography **27**(2). doi: 10.1029/2012PA002283

Doornenbal, H. & Stevenson, A., 2010. Petroleum geological atlas of the Southern Permian Basin area. EAGE.

Droser, M.L. & Bottjer, D.J., 1986. A semiquantitative field classification of ichnofabric. Journal of Sedimentary Research **56**(4).

Dusar, M., Langenaeker, V. & Wouters, L., 2001. Permian-Triassic–Jurassic lithostratigraphic units in the Campine basin and the Roer Valley Graben (NE Belgium). Geologica Belgica.

Elsayed, N., 2021, May 27. Small- and Large-Scale Sedimentological Processes in the Early Jurassic Mud- Dominated Successions, Cleveland Basin, UK. Retrieved 16 April 2024, from [Thesis]. Manchester, UK: The University of Manchester; 2021. website: https://www.escholar.manchester.ac.uk/uk-ac-man-scw:328852

Figueiredo, A.G., Sanders, J.E. & Swift, D.J.P., 1982. Storm-graded layers on inner continental shelves: Examples from southern Brazil and the Atlantic coast of the Central United States. Sedimentary Geology **31**(3): 171–190. doi: 10.1016/0037-0738(82)90057-4

Fisher, I.S.J., 1986. Pyrite replacement of mollusc shells from the Lower Oxford Clay (Jurassic) of England. Sedimentology **33**(4): 575–585. doi: 10.1111/j.1365-3091.1986.tb00762.x

French, K.L., Sepúlveda, J., Trabucho-Alexandre, J., Gröcke, D.R. & Summons, R.E., 2014. Organic geochemistry of the early Toarcian oceanic anoxic event in Hawsker Bottoms, Yorkshire, England. Earth and Planetary Science Letters **390**: 116–127. doi: 10.1016/j.epsl.2013.12.033

Geluk, M.C., Duin, E.J.Th., Dusar, M., Rijkers, R.H.B., van den Berg, M.W. & van Rooijen, P., 1994. Stratigraphy and tectonics of teh Roer Valley Graben. Geologie En Mijnbouw (73): 129–141.

Geluk, M.C., Duin, E.T., Dusar, M., Rijkers, R.H.B., Van den Berg, M.W. & Van Rooijen, P., 1995. Stratigraphy and tectonics of the Roer Valley Graben. Geologie En Mijnbouw **73**: 129–129.

Hemingway, J.E., 1974. The geology and mineral resources of Yorkshire. Yorkshire Geological Society 161–233.

Herngreen, G.F.W., Kouwe, W.F.P. & Wong, T.E., 2003. The Jurassic of the Netherlands. GEUS Bulletin **1**: 217–230. doi: 10.34194/geusb.v1.4652

Hesselbo, S.P., Gröcke, D.R., Jenkyns, H.C., Bjerrum, C.J., Farrimond, P., Morgans Bell, H.S. & Green, O.R., 2000. Massive dissociation of gas hydrate during a Jurassic oceanic anoxic event. Nature **406**(6794): 392–395. doi: 10.1038/35019044

Huber, N.K., 1958. The environmental control of sedimentary iron minerals. Economic Geology **53**(2): 123–140. doi: 10.2113/gsecongeo.53.2.123

Ivimey–Cook, H.C. & Powell, J.H., 1991. Late Triassic and early Jurassic biostratigraphy of the Felixkirk Borehole, North Yorkshire. Yorkshire Geological Society **48**: 367–374.

Jenkyns, H.C., 1988. The early Toarcian (Jurassic) anoxic event – stratigraphic, sedimentary, and geochemical evidence. American Journal of Geoscience (288): 101–151.

Kemp, D.B., Coe, A.L., Cohen, A.S. & Schwark, L., 2005. Astronomical pacing of methane release in the Early Jurassic period. Nature **437**(7057): 396–399. doi: 10.1038/nature04037

Lazar, O.R., Bohacs, K.M., Macquaker, J.H.S., Schieber, J. & Demko, T.M., 2015. Capturing Key Attributes of Fine-Grained Sedimentary Rocks In Outcrops, Cores, and Thin Sections: Nomenclature and Description Guidelines. Journal of Sedimentary Research **85**(3): 230–246. doi: 10.2110/jsr.2015.11

Legrand, R., 1961. L'épeirogenèse, source de tectonique, d'aprés des examples choisis en Belgique. Mémories de l'Insitut Géologique de l'Université de Louvain **22**: 66.

Loope, D.B., Kettler, R.M., Weber, K.A., Hinrichs, N.L. & Burgess, D.T., 2012. Rinded iron-oxide concretions: hallmarks of altered siderite masses of both early and late diagenetic origin. Sedimentology **59**(6): 1769–1781. doi: 10.1111/j.1365-3091.2012.01325.x

Lott, G.K., Wong, T.E., Dusar, M., Andsbjerg, J., Mönnig, E., Feldman-Olszewska, A. & Verreussel, R.M.C.H., 2010. Jurassic. In: Doornenbal, J.C. and Stevenson, A.G. (editors): Petroleum Geological Atlas of the Southern Permian Basin Area. EAGE Publications 175–193.

Love, L.G. & Amstutz, G.C., 1966. Review of Micro- scopic Pyrite from the Devonian Chattanooga Shale and Rammelsberg Banderz; Fortschr. Mineral **43**(273–309).

Luijendijk, E., Van Balen, R.T., Ter Voorde, M. & Andriessen, P.A.M., 2011. Reconstructing the Late Cretaceous inversion of the Roer Valley Graben (southern Netherlands) using a new model that integrates burial and provenance history with fission track thermochronology. Journal of Geophysical Research **116**(B6): B06402. doi: 10.1029/2010JB008071

Macquaker, J.H., Taylor, K.G. & Gawthorpe, R.L., 2007. High-resolution facies analyses of mudstones: implications for paleoenvironmental and sequence stratigraphic interpretations of offshore ancient mud-dominated successions. Journal of Sedimentary Research **77**(4): 324–339.

McArthur, J.M., Donovan, D.T., Thirlwall, M.F., Fouke, B.W. & Mattey, D., n.d. Strontium isotope proȼle of the early Toarcian (Jurassic) oceanic anoxic event, the duration of ammonite biozones, and belemnite palaeotemperatures. Earth and Planetary Science Letters.

Mitchell, A.J., Allison, P.A., Gorman, G.J., Piggott, M.D. & Pain, C.C., 2011. Tidal circulation in an ancient epicontinental sea: The Early Jurassic Laurasian Seaway. Geology **39**(3): 207–210. doi: 10.1130/G31496.1

Mozley, P.S., 1989. Relation between depositional environment and the elemental composition of early diagenetic siderite. Geology **17**(8): 704. doi: 10.1130/0091-7613(1989)017<0704:RBDEAT>2.3.CO;2

NAM & RGD, 1980. Stratigraphic nomenclature of The Netherlands. Erhandelingen van Het Koninklijk Nederlands Geologisch Mijnbouwkundig Genootschap (32): 77.

O'B Knox, R.W., 1984. Lithostratigraphy and depositional history of the late Toarcian sequence at Ravenscar, Yorkshire. Yorkshire Geological Society **45**(1–2): 99–108.

O'Brien, N.R., 1990. Significance of lamination in Toarcian (Lower Jurassic) shales from Yorkshire, Great Britain. Sedimentary Geology **67**(1–2): 25–34. doi: 10.1016/0037-0738(90)90025-O

O'Brien, N.R., 1996. Shale lamination and sedimentary processes. Geological Society, London, Special Publications **116**(1): 23–36.

OERTEL, G. & CURTIS, C.D., 1972. Clay-Ironstone Concretion Preserving Fabrics Due to Progressive Compaction. GSA Bulletin **83**(9): 2597–2606. doi: 10.1130/0016-7606(1972)83[2597:CCPFDT]2.0.CO;2

Ondrak, R., Foerster, A., Scheck, M. & Gerisch, R., 1999. The present-day temperature field of the Northeast German Basin - A comparison of temperature measurements and 3D-modeling. Sciences Géologiques, Bulletins et Mémoires **99**(1): 111–114.

Potter, P.E., Maynard, J.B. & Depetris, P.J., 2005. Mud and Mudstones: Introduction and Overview. Springer Science & Business Media: 305 pp.

Powell, J.H., 1984. Lithostratigraphical nomenclature of the Lias Group in the Yorkshire Basin. Yorkshire Geological Society **45**: 51–57.

Powell, J.H., 2010. Jurassic sedimentation in the Cleveland Basin: a review. Proceedings of the Yorkshire Geological Society **58**(1): 21–72. doi: 10.1144/pygs.58.1.278

Prothero, D.R. & Schwab, F., 1996. An introduction to sedimentary rocks and stratigraphy. Sedimentary Geology, New York, WH Freeman and Company **575**.

Pye, K. & Krinsley, D.H., 1986. Microfabric, mineralogy and early diagenetic history of the Whitby Mudstone Formation (Toarcian), Cleveland Basin, U.K. Geological Magazine **123**(3): 191–203. doi: 10.1017/S0016756800034695

Rawson, P.F. & Wright, J.K., 1992. RAWSON, P. F. & WRIGHT, J. K. 1992. The Yorkshire Coast. Geologists' Association Guide **34**.

Rawson, P.F. & Wright, J.K., 1995. Jurassic of the Cleveland Basin, North Yorkshire. In Taylor, P D (ed.) Field Geology of the British Jurassic. Geological Society of London 173–208.

Rawson, P.F. & Wright, J.K., 1996. Jurassic of the Cleveland Basin, North Yorkshire. In: TAYLOR, P. D. (ed.) Field Geology of the British Jurassic. Geological Society, London 173–208.

Rawson, P.F. & Wright, J.K., 2000. The Yorkshire Coast, 3 ed. Geologists' Association Guide.

Rickard, D., 2012. Chapter 6 - Sedimentary Pyrite. *In*: D. Rickard (ed.): Developments in Sedimentology. Elsevier: pp. 233–285. doi: 10.1016/B978-0-444-52989-3.00006-4

Roberts, J.A., Kenward, P.A., Fowle, D.A., Goldstein, R.H., González, L.A. & Moore, D.S., 2013. Surface chemistry allows for abiotic precipitation of dolomite at low temperature. Proceedings of the National Academy of Sciences **110**(36): 14540–14545. doi: 10.1073/pnas.1305403110

Sageman, B.B., Murphy, A.E., Werne, J.P., Ver Straeten, C.A., Hollander, D.J. & Lyons, T.W., 2003. A tale of shales: the relative roles of production, decomposition, and dilution in the accumulation of organic-rich strata, Middle–Upper Devonian, Appalachian basin. Chemical Geology **195**(1): 229–273. doi: 10.1016/S0009-2541(02)00397-2

Schieber, J., 1999. Distribution and deposition of mudstone facies in the Upper Devonian Sonyea Group of New York. Journal of Sedimentary Research **69**(4): 909–925. doi: 10.2110/jsr.69.909

Schieber, J., 2011. Reverse engineering mother nature — Shale sedimentology from an experimental perspective. Sedimentary Geology **238**(1): 1–22. doi: 10.1016/j.sedgeo.2011.04.002

Schieber, J. & Southard, J.B., 2009. Bedload transport of mud by floccule ripples—Direct observation of ripple migration processes and their implications. Geology **37**(6): 483–486. doi: 10.1130/G25319A.1

Schieber, J. & Yawar, Z., 2009. A new twist on mud deposition-mud ripples in experiment and rock record. The Sedimentary Record **7**(2): 4–8.

Sel, O., Radha, A.V., Dideriksen, K. & Navrotsky, A., 2012. Amorphous iron (II) carbonate: Crystallization energetics and comparison to other carbonate minerals related to CO2 sequestration. Geochimica et Cosmochimica Acta **87**: 61–68. doi: 10.1016/j.gca.2012.03.011

Simms, M.J., Chidlaw, N., Morton, N. & Page, K.N., 2004. British lower Jurassic stratigraphy. Geological Conservation Review **30**: 458.

SMITH, W., 1797. SMITH, W. 1797. MSS published by DOUGLAS, J.A. and COX, L.R. (1949). An early list of strata by William Smith. Geological Magazine, 86, 180-188.

Trabucho-Alexandre, J., 2015. More gaps than shale: erosion of mud and its effect on preserved geochemical and palaeobiological signals. London: The Geological Society of London.

Trabucho-Alexandre, J., Dirkx, R., Veld, H., Klaver, G. & De Boer, P.L., 2012. Toarcian Black Shales In the Dutch Central Graben: Record of Energetic, Variable Depositional Conditions During An Oceanic Anoxic Event. Journal of Sedimentary Research **82**(2): 104–120. doi: 10.2110/jsr.2012.5

Trabucho-Alexandre, J.P., Gröcke, D.R., Atar, E., Herringshaw, L. & Jarvis, I., 2022. A new subsurface record of the Pliensbachian–Toarcian, Lower Jurassic, of Yorkshire. Proceedings of the Yorkshire Geological Society **64**(2): pygs2022-007. doi: 10.1144/pygs2022-007

van Adrichem Boogaert, H.A. & Kouwe, W.F.P., 1994. Stratigraphic nomenclature of the Netherlands, revision and update by RGD and NOGEPA. Mededelingen Rijks Geologische Dienst **50**(sections A–J).

Van Lith, Y., Warthmann, R., Vasconcelos, C. & McKenzie, J.A., 2003. Microbial fossilization in carbonate sediments: a result of the bacterial surface involvement in dolomite precipitation. Sedimentology **50**(2): 237–245. doi: 10.1046/j.1365-3091.2003.00550.x

Wang, L., Shi, X. & Jiang, G., 2012. Pyrite morphology and redox fluctuations recorded in the Ediacaran Doushantuo Formation.

Palaeogeography, Palaeoclimatology, Palaeoecology **333–334**: 218–227. doi: 10.1016/j.palaeo.2012.03.033

Wignall, P.B. & Newton, R., 1998. Pyrite framboid diameter as a measure of oxygen deficiency in ancient mudrocks. American Journal of Science, 298(7), 537-552. American Journal of Science **298**(7): 537–552.

Wilkin, R.T., Arthur, M.A. & Dean, W.E., 1997. History of water-column anoxia in the Black Sea indicated by pyrite framboid size distributions. Earth and Planetary Science Letters **148**(3): 517–525. doi: 10.1016/S0012-821X(97)00053-8

Wilkin, R.T., Barnes, H.L. & Brantley, S.L., 1996. The size distribution of framboidal pyrite in modern sediments: An indicator of redox conditions. Geochimica et Cosmochimica Acta **60**(20): 3897–3912. doi: 10.1016/0016-7037(96)00209-8

Wilson, R.D. & Schieber, J., 2014. Muddy Prodeltaic Hyperpycnites In the Lower Genesee Group of Central New York, USA: Implications For Mud Transport In Epicontinental Seas. Journal of Sedimentary Research **84**(10): 866–874. doi: 10.2110/jsr.2014.70

Wilson, V., Hemingway, J.E. & Black, M., 1934. A synopsis of the jurassic rocks of yorkshire. Proceedings of the Geologists' Association **45**(3): 247-IN3. doi: 10.1016/S0016-7878(34)80023-5

Winstanley, A.M., 1993. A review of the Triassic play in the Roer Valley Graben, SE onshore Netherlands. Geological Society, London, Petroleum Geology Conference Series **4**(1): 595–607.

Wong, T.E., 2007. Jurassic. In: Geology of the Netherlands. Amsterdam, Royal Netherlands Academy of Arts and Sciences 107–125.

Worum, G., Michon, L., Vanbalen, R., Vanwees, J., Cloetingh, S. & Pagnier, H., 2005. Pre-Neogene controls on present-day fault activity in the West Netherlands Basin and Roer Valley Rift System (southern Netherlands): role of variations in fault orientation in a uniform low-stress regime. Quaternary Science Reviews **24**(3–4): 473–488. doi: 10.1016/j.quascirev.2004.02.020

Yawar, Z. & Schieber, J., 2017. On the origin of silt laminae in laminated shales. Sedimentary Geology **360**: 22–34. doi: 10.1016/j.sedgeo.2017.09.001

Ziegler, P.A., 1988. Evolution of the Artic North Atlantic and the western Tethys. Am. Assoc. Pet. Geol. Mem **43**: 1–198.

Ziegler, P.A., 1990. Geological Atlas of Western and Central Europe. Shell International Petroleum (Geological Society, London).

Ziegler, P.A., 1992. European Cenozoic rift system. Tectonophysics **208**(1–3): 91–111.

Zijerveld, L., Stephenson, R., Cloetingh, S.A.P.L., Duin, E. & Van den Berg, M.W., 1992. Subsidence analysis and modelling of the Roer Valley Graben (SE Netherlands). Tectonophysics **208**(1–3): 159–171.